2008-07-30

Spectroscopic Study of Compressible Mobile Phase and Stationary Phase Behavior in Chromatography

Lawrence R. Baker
Brigham Young University - Provo

Spectroscopic Study of Compressible Mobile Phase and Stationary Phase Behavior in Chromatography

by

Lawrence Robert Baker

A thesis submitted to the faculty of

Brigham Young University

in partial fulfillment of the requirements for the degree of

Master of Science

Department of Chemistry and Biochemistry

Brigham Young University

December 2008

BRIGHAM YOUNG UNIVERSITY

GRADUATE COMMITTEE APPROVAL

of a thesis submitted by

Lawrence Robert Baker

This thesis has been read by each member of the following graduate committee and by majority vote has been found to be satisfactory.

Date	James E. Patterson, Chair
Date	Steven R. Goates
Date	Matthew C. Asplund
Date	Milton L. Lee

BRIGHAM YOUNG UNIVERSITY

As chair of the candidate's graduate committee, I have read the thesis of Lawrence Robert Baker in its final form and have found that (1) its format, citations, and bibliographical style are consistent and acceptable and fulfill university and department style requirements; (2) its illustrative materials including figures, tables, and charts are in place; and (3) the final manuscript is satisfactory to the graduate committee and is ready for submission to the university library.

Date	James E. Patterson Chair, Graduate Committee

Accepted for the Department

Date	David V. Dearden, Professor

Accepted for the College

Date	Thomas W. Sederberg, Associate Dean College of Physial & Mathematical Sciences

ABSTRACT

Spectroscopic Study of Compressible Mobile Phase and Stationary Phase Behavior in Chromatography

Lawrence Robert Baker

Department of Chemistry and Biochemistry

Master of Science

Raman spectroscopy, laser-induced fluorescence, and sum-frequency generation (SFG) spectroscopy are used to investigate the behavior of compressible mobile phases and stationary phases under a variety of chromatographic conditions. Efforts to understand and optimize separations employing compressible mobile phases have been limited by a lack of understanding of the mobile phase density gradient. Mobile phase compressibility leads to gradients in linear velocity and solute retention and affects separation speed and efficiency, especially in packed columns. This work describes on-column density measurement of CO_2, a common carrier fluid for SFC and SGC, in packed capillary columns using Raman microspectroscopy. On-column detection by laser-induced fluorescence is used to observe the effect of the mobile phase density gradient on separation speed and efficiency, and experimental efficiency is compared to a theoretical model. Additionally, SFG spectroscopy allows for probing the structure of

model monomeric and polymeric C18 stationary phases under pressure; this provides a basis for correlating selectivity with pressure-induced structural changes in stationary phase materials. Together, this work provides a more complete understanding of the role of column pressure and fluid compressibility on the speed, efficiency, and selectivity of chemical separations.

ACKNOWLEDGEMENTS

I express gratitude to my wife, Catherine, to my daughter, Eliza, and to my parents and siblings who have desired for my success in this program and have motivated me to always do my best. I am also very grateful for Dr. Goates who has been an amazing advisor, mentor, and friend. If it were not for him, I would not be going into chemistry. I will miss you very much. I am additionally grateful to Dr. Patterson, with whom it has been a privilege to work and from whom I have learned much. I have also enjoyed the association of many good friends that have made my experiences here fun and meaningful. It is difficult to express how much these friendships have meant to me. I also express appreciation to my teachers and those that have helped me with this work, including Dr. Matthew Asplund, Dr. Juliana Boerio-Goates, and Dr. Milton Lee.

Table of Contents

Introduction

Chromatography is commonly used for both analytical and preparative separations in a wide range of fields. Applications of chromatography include separation and purification of pharmaceuticals, protein and peptide separations for the detection of biomarkers, environmental monitoring, and detection of warfare agents for national defense. The focus of the medical industry has been toward genetic based medicine, and advances in this field depend on the identification of biomarkers for early disease detection and treatment. This field especially has fueled the need for fast separation techniques capable of high-throughput analyses. Regardless of the application, advances in separation science depend on a fundamental understanding of the processes that determine the speed, efficiency, and selectivity of a separation. The purpose of this work is to better understand the behavior of compressible mobile phases and stationary phases. This fundamental understanding provides a basis for improving the performance of chromatographic separations.

Chromatographic techniques can be characterized by the type of mobile phase and type of stationary phase they use. Gases, liquids, or supercritical fluids can be used as mobile phases for separations. Stationary phases are classified as normal phase, meaning more polar than the mobile phase, or reversed phase, meaning less polar than the mobile phase. For the separation of small organic molecules, proteins, and peptides, reversed phases are by far the most common.

Gas chromatography (GC) is more efficient at high flow rates than liquid chromatography (LC) or supercritical fluid chromatography (SFC) because gases allow for higher rates of diffusion than other fluids. The slower the rate of diffusion, the longer

it takes analyte to migrate through the mobile phase to the stationary phase. This gives rise to deviations from equilibrium partitioning of the band between the mobile and stationary phases as it moves through the column and results in band broadening. For fluids with slow diffusion, the critical diameter of the column must be small to maintain high efficiency at fast flow rates. The critical diameter of a column refers to the distance that an analyte molecule must migrate through the mobile phase before reaching the stationary phase. Packed columns allow for smaller critical diameters than open tubular columns, but column packing also creates resistance to mobile phase flow. Consequently, higher inlet pressures are needed to generate flow in packed columns than open tubular columns, and the pressure drop along packed columns can be significantly higher than pressure drops in open columns.

Because of high diffusion rates in gases, GC is usually performed in open columns. However, open tubular LC is impractical because of the large critical diameter of an open column and the slow rates of diffusion in liquids. Consequently, high performance liquid chromatography (HPLC) is performed on columns packed with microparticles to ensure a small critical diameter of the column. Because of resistance to flow through such a tightly packed column, high inlet pressures are common in HPLC. These inlet pressures are characteristically between 5000 and 10 000 psi.

Although GC is usually faster and much more efficient than LC, it is limited to the analysis of volatile compounds. As compounds increase in size, their volatility decreases, making large compounds difficult to analyze by GC. Because of the solvating power of liquids, even large compounds are readily analyzed by LC if they are partially

soluble in the mobile phase. Consequently, LC is applicable to the analysis of a much broader range of compounds than GC.

SFC represents a compromise between the solvating power of LC and the high rates of diffusion in GC. Although more viscous than a gas, a supercritical fluid is much less viscous than a liquid, allowing for fairly fast rates of diffusion. Additionally, the solvating power of supercritical fluids at high density can decrease analyte retention, making SFC capable of analyzing a wider range of compounds than GC. SFC is done in both open tubular and packed columns. When packed columns are used, a larger pressure drop across the column is needed to overcome the resistance to flow. However, due to the low viscosity of supercritical fluids, higher flow rates are possible in SFC than in HPLC. Because supercritical fluids are compressible, the column pressure drop results in expansion of the mobile phase. Because the solvating power of a supercritical fluid depends strongly on density, the retention of analyte can change as it moves down the column. Additionally, because the mass flow rate is constant through the column, the loss of density also results in faster flow of the mobile phase.

In SFC, a flow restrictor is used at the column outlet to maintain column pressure. In the absence of a flow restrictor, the column outlet pressure can drop below the critical pressure of the fluid. This technique is known as solvating gas chromatography (SGC) and can be thought of as a hybrid method between SFC and GC. Fast, high efficiency separations have been demonstrated using SGC, despite many reports in the literature that have shown a loss of efficiency in SFC with large pressure drops. Rather than viewing SGC as an SFC column operating over a large pressure drop, the low density region of an SGC column can be described as packed-column GC, where the combination of high

diffusion rates and a small critical column diameter result in fast, high efficiency separations.

One of the goals of this research has been to understand the flow behavior of a compressible mobile phase in a packed column operating across a large pressure drop and how this flow behavior affects separation speed and efficiency. The first three chapters of this thesis are devoted to a study of this question. These chapters describe direct measurements of mobile phase flow in an SGC column using Raman spectroscopy, and its effects on separation speed and efficiency as observed on-column by laser-induced fluorescence. To the best of my knowledge, these experiments represent the first on-column observations of mobile phase flow and analyte retention in chromatography. The first three chapters are being submitted for publication in Applied Spectroscopy (Chapter 1) and Journal of Chromatography A (Chapters 2 and 3). Chapters 2 and 3 include the results of on-column, laser-induced fluorescence measurements of analyte elution and band dispersion. These measurements were taken by Marisa Stark and were initially reported in her Master's Thesis. However, I have performed significant analysis of her results, and knowledge of the mobile phase flow behavior has provided important additional insights into her work. Consequently, it is appropriate to include Marisa's results with a discussion of their significance in this thesis. Local efficiency calculations and modeling are extensions of Marisa's work that I have performed.

Research has also been performed to understand the effects of pressure on the structure of stationary phase materials. The shape selectivity of stationary phases is known to be closely linked to structure. Although HPLC and SFC are performed at high pressures, little work has been done to characterize the effects of pressure on stationary

phase structure, even though the literature reports several examples of pressure-induced changes in stationary phase selectivity. Chapter 4 of this thesis describes structural measurements of model stationary phases at pressures up to 60 atm using sum-frequency generation spectroscopy. These observations provide a basis for correlating column pressure with selectivity in LC and SFC separations.

Chapter 1: Characterization of Carbon Dioxide Mobile Phase Density Profiles in Packed Capillary Columns by Raman Microscopy

Abstract

Efforts to understand and optimize separations employing compressible mobile phases have been limited by a lack of understanding of the mobile phase density gradient. Mobile phase compressibility leads to gradients in linear velocity and solute retention and affects separation speed and efficiency, especially in packed columns. Gas chromatography (GC), supercritical fluid chromatography (SFC), and solvating gas chromatography (SGC) each rely on compressible mobile phases. This work describes on-column density measurement of CO_2, a common carrier fluid for SFC and SGC, in packed capillary columns using Raman microspectroscopy of the position of the Fermi doublet. Correlation of the spectrum with density was calibrated over a pressure range of 15 to 290 atm at 125 and 150 °C, which then allowed for determination of the density gradient of fluid flowing through a packed capillary column. The results of this work will be used to model the flow behavior of compressible fluids to understand the effects of mobile phase compressibility on separation speed and efficiency.

Introduction

Gas chromatography (GC), supercritical fluid chromatography (SFC), and solvating gas chromatography (SGC) use compressible fluids as the mobile phase for separations. In these techniques, fluid compressibility results in on-column expansion of the mobile phase leading to column density gradients. In SFC and SGC, local retention factors and plate heights are strongly dependent on mobile phase density [1–6]. In SFC,

axial column density gradients are kept small by the use of a flow restrictor at the column outlet; in SGC, the absence of a flow restrictor results in higher mobile phase linear velocities and much steeper density gradients which span the supercritical fluid to gas transition [7]. Several attempts have been made to model the flow of compressible mobile phases, [3, 8–9] but these models have not been verified by experimental density measurements. On-column measurements of the mobile phase density gradient enable testing of theoretical models of mobile phase flow behavior and provide a better understanding about the effects of mobile phase compressibility on solute retention factors and local plate heights in compressible mobile phase separations.

CO_2 is a common mobile phase for SFC and SGC because of its low critical temperature (31.1 °C), good solvating power, and low toxicity. Because CO_2 is centrosymmetric, its vibrational modes can be either Raman or IR active, but not both. The symmetric stretch is Raman active while the bending mode is IR active. However, the symmetric stretch has Σ_g^+ symmetry, and the first overtone of the bend is composed of two states with Δ_g and Σ_g^+ symmetries. The shared Σ_g^+ symmetry allows these vibrational modes to couple; because the energy of the symmetric stretch is accidentally degenerate with the first overtone of the bending mode, coupling is strong. This is known as Fermi Resonance [10–11] and is observed in the Raman spectrum as a doublet with peaks centered at about 1286 and 1389 cm^{-1} (see Figure 1).

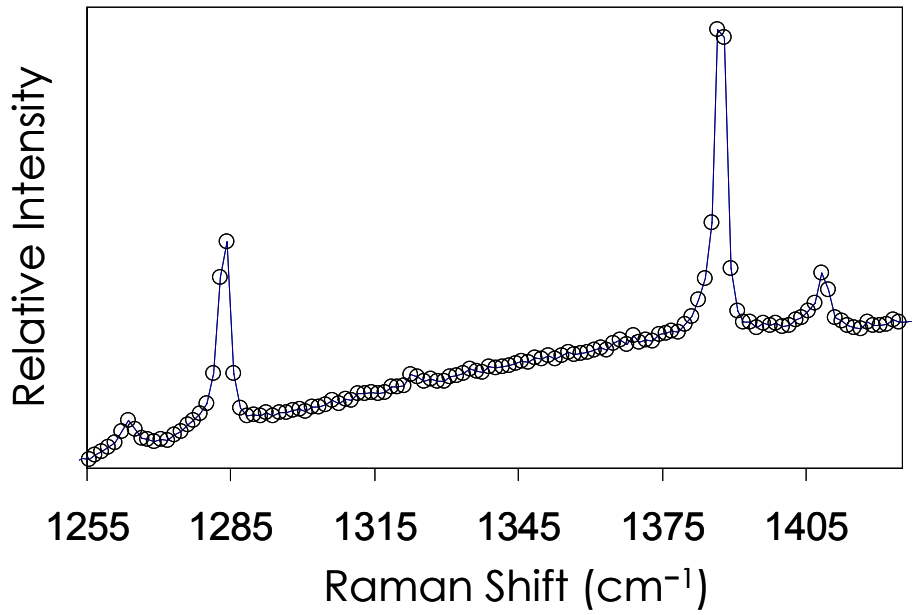

Figure 1 Raman spectrum of the Fermi doublet in CO_2. The band to the left, centered near 1286 cm^{-1}, is the ν_1 transition, and the band to the right, centered near 1389 cm^{-1}, is the $2\nu_2$ transition. The smaller peaks on the outside of the spectrum are the hot bands. This spectrum was obtained in a packed capillary at 125 °C and 170 atm.

Wright and Wang [12] studied the frequency shift of the Fermi doublet as a function of density; they observed that the frequencies of the 1286 cm^{-1} (ν_1) transition and the 1389 cm^{-1} ($2\nu_2$) transition decreased with increasing density at a rate of 5.74 $cm^{-1}/(g\ cm^{-3})$ and 2.90 $cm^{-1}/(g\ cm^{-3})$, respectively. They also studied [13] the effects of density on the relative intensities of the two bands in the Fermi doublet. The ν_1 intensity was found to decrease relative to the $2\nu_2$ intensity at increasing densities in the polarized bands; however, this effect is greatly diminished in the depolarized bands. Wright and Wang additionally showed [14] that the width of the rotational envelope in the low-frequency Raman spectrum correlates to density.

Garrabos et al. [15–17] further investigated the density dependence of the Fermi doublet in CO_2. They reproduced the results of Wright and Wang and obtained data in the critical density region that Wright and Wang had been unable to observe. Several other Raman studies have correlated density to spectral changes in CO_2 [18–20]. However, as with the studies mentioned above, these experiments have been aimed at physical studies of CO_2 rather than as a means to probe fluid density.

In this work, I demonstrate the viability of Raman microscopy for determining the mobile phase density in packed capillary columns. This work represents the first on-column measurements of mobile phase density and allows for testing theoretical models of mobile phase flow behavior in packed column chromatography. Because SGC operates over a much steeper density gradient than SFC, SGC is a useful model for observing the effects of fluid compressibility on separation speed and efficiency. Consequently, this study focuses on measuring the density gradient in an SGC column.

Experimental

An illustration of the experimental setup is shown in Figure 2. Raman spectra of CO_2 were collected directly on-column using a Raman microscope (Chromex 2000). The capillary column was fused silica and contained a polyimide coating for reinforcement. To probe inside the capillary, segments of the polyimide coating were removed to form windows. A home built heating plate that fit on the stage of the Raman microscope allowed for temperature control of the column.

To calibrate this method, Raman spectra were collected at known densities by closing the column outlet and allowing the entire column to pressurize. To obtain the density profile of the dynamic mobile phase in an SGC column, the column outlet was opened, and spectra were collected at increments along the column.

Segments of the polyimide coating were removed using hot sulfuric acid. Glass slides were placed on the heating plate to insulate the column. The temperature of the heating plate was regulated with an adjustable DC supply and monitored by a T type thermocouple. The thermocouple was calibrated against the melting points of Sn and Ga and the melting and boiling points of water (18 MΩ). Heat transfer to the microscope platform was minimized by insulating the stage with foam tape. Monitoring showed that the temperature across the column was stable to ±3 °C.

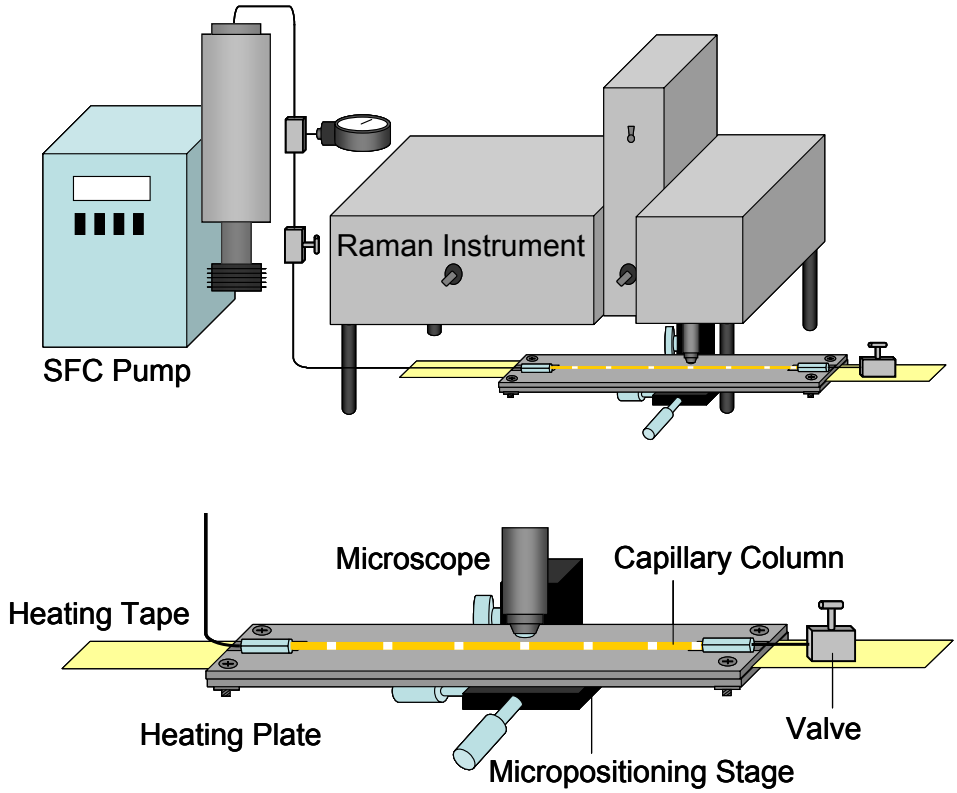

Figure 2 Capillary column and heating plate on the microscope stage. The SFC pump is equipped with a digital pressure transducer and can be set to maintain a constant inlet pressure. An analog pressure gauge serves to verify accuracy of the digital transducer. For calibration runs, a known pressure is achieved by closing the needle valve at the column outlet and allowing the entire column to pressurize. Opening the outlet valve allows probing the column density gradient under SGC conditions.

The column was prepared using 5-μm Nucleosil silica spheres (Macherey-Nagel) with a pore size of 100 Å. A 2-μm steel screen (Valco) housed inside the union at the column outlet supported the particles. The column was packed at 300 atm using the slurry packing method described by Malik et al. [21]. Columns were 50 cm long and had an inner diameter of 200 μm.

The original 785 nm light source of the Chromex instrument failed and was replaced with the 488 nm line from an argon ion laser (Lexel 95). Figure 3 shows the excitation and collection optics of the Raman spectrometer as modified for my work. A dichroic beam splitter (Semrock Optics, FF500-Di01) served to remove extraneous laser emissions that interfere with the observation of Stokes-shifted peaks. The dichroic beam splitter and a holographic notch filter (Kaiser Optical Systems, 18015) filtered the Rayleigh line from the Raman signal.

Integration times were chosen to achieve 75 percent saturation of the CCD. Multiple sets were then summed to obtain a five-minute integration time for each run. The laser power was kept between 200 and 350 mW to avoid perturbing the density by laser-induced heating. To verify that the laser did not affect fluid density, I collected spectra at powers as low as 50 mW and observed no change in fluid density as a function of laser power. Additionally, throughout the experiment I regularly reduced the laser power to 75 mW; comparison of the data collected at this reduced power showed no significant deviation from my other data.

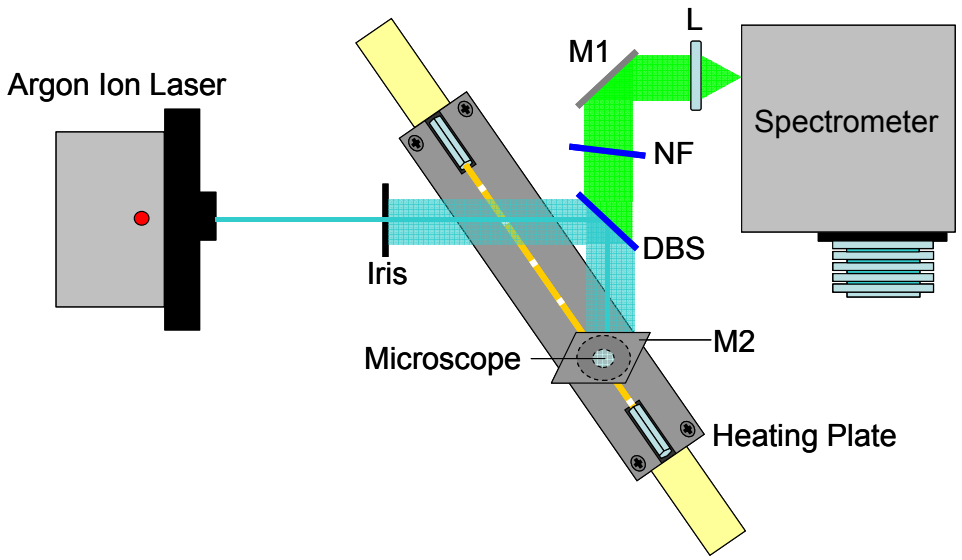

Figure 3 Modified beam path of the Chromex 2000 Raman microscope. M1 and M2 are mirrors; L is the f-matching lens to the spectrometer; NF is a 488 nm holographic notch filter; and DBS is a dichroic beam splitter.

Figure 4 shows the capillary lying in the groove in the heating plate imaged at low magnification. Raman spectra were collected using a 20× 0.4 N.A. microscope objective. Imaging the column using this objective showed that the laser spot size was just smaller than the 35 μm slit width of the spectrometer.

Spectra were processed using Grams/32 (Galactic Industries Co.) software. Due to instrument limitations, relatively few data points were collected across the bands of the Fermi doublet. However, fitting these bands to Gaussian functions allowed me to determine the peak centers with resolution greater than the pixel limitation of the instrument. Density values were obtained by solving the Jacobsen-Stewart modification of the Benedict-Webb-Rubin (BWR) equation of state [22].

Results and Discussion

In my preliminary experiments, I collected Raman spectra of CO_2 in an open tubular capillary. I reproduced the results of Wright and Wang [13] and Garrabos et al. [17] by correlating density to the relative intensity of the ν_1 and $2\nu_2$ bands. However, when the experiment was repeated with a silica-packed capillary, I found that multiple reflections off the silica packing scramble the polarization of the excitation beam as well as the Raman scatter. Loss of polarization makes it impossible to distinguish between the isotropic and anisotropic Raman signal. Because the effect of density on the relative intensity of the ν_1 and $2\nu_2$ bands is greatly diminished in the depolarized signal, I was unable to measure fluid density in a packed column using the relative intensity of the Fermi doublet.

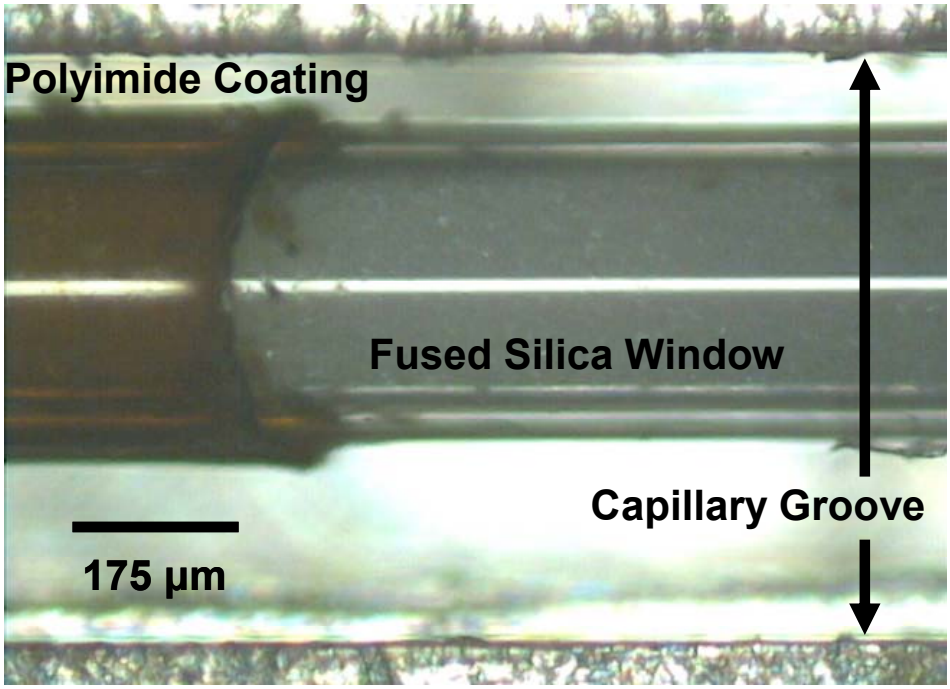

Figure 4 Packed capillary column (350 µm o.d., 200 µm i.d.) in the groove of the heating plate imaged under low magnification. To allow probing inside the fused silica capillary, a segment of the polyimide coating was removed to form a window. The bright line in the center of the capillary is a reflection from the light source of the microscope.

Although the loss of polarization in a packed column prevents fluid density measurements based on relative intensities, the effect of density on the frequency of the Fermi doublet is independent of polarization. The frequency of the ν_1 band changes with fluid density at nearly twice the rate of the $2\nu_2$ band, so in principle, the most sensitive calibration for fluid density would be based on the absolute frequency of the ν_1 band. However, density measurements based on absolute frequencies proved unreliable due to spectral drift of the spectrometer. Because the frequencies of the ν_1 and $2\nu_2$ bands respond to density at different rates, I was able to correct for spectral drift by measuring the difference in frequency between these two bands. Although this method is less sensitive than measuring density based on absolute frequencies, by normalizing against spectral drift, it provided the most accurate method for density determination.

For brevity, I define δ as the difference in frequency between the ν_1 and $2\nu_2$ bands. Figure 5A shows a plot of δ as function of CO_2 density in a packed column. These densities represent a pressure range of 15 to 290 atm at 125 and 150 °C. Fitting the bands to Gaussian functions yielded accurate values for δ. This is verified by the response of δ to changes in fluid density. Based on a least squares regression of the linear region above 0.1 g cm^{-3}, the 95% confidence level for uncertainty in δ is 0.06 cm^{-1}. This is much better than the pixel resolution of the spectrometer which is 1.4 cm^{-1} and shows that curve fitting significantly enhanced the sensitivity of my measurements.

I initially attempted to use the linear fit for δ to determine on-column densities, but this consistently resulted in negative density values near the column outlet. This prompted me to collect additional spectra of CO_2 at low densities. These runs showed that at low density the response of δ becomes increasingly sensitive. This is illustrated in

Figure 5B where the dashed line represents an extrapolation of the linear fit of the high density data (greater than 0.1 g cm^{-1}), and the solid line represents a quadratic fit to the low density data (less than 0.1 g cm^{-1}). I do not know if this curvature at low density is intrinsic behavior of gaseous CO_2 or if it is an artifact of the experiments. However, fitting spectra with a δ value greater than 102.9 cm^{-1} to the linear calibration curve and spectra with a lower δ value to the quadratic calibration curve produced physically meaningful SGC density profiles. An example of a measured SGC profile is shown in Figure 6. The error bars represent 95% confidence intervals. The accuracy of the profile is further verified by the close alignment of the measured densities with the known column inlet density. In a later paper, I also show that this density profile can be modeled theoretically with a high level of accuracy.

As an interesting side note, I observed that the Raman intensity in the packed column was greater than the signal intensity from an open tubular column. This is counterintuitive because the volume of CO_2 is significantly smaller in a packed column. I hypothesize that this increase in signal is due to an increase in effective path length of the excitation beam due to multiple reflections off the silica packing.

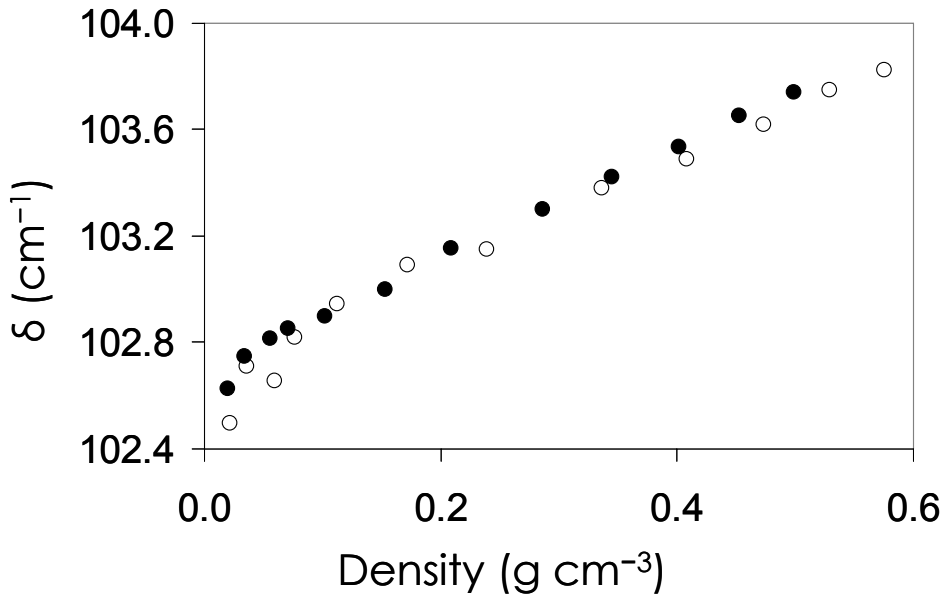

Figure 5A Calibration curve based on the difference in frequency between the ν_1 and $2\nu_2$ bands (δ) as a function of carbon dioxide density. Data collected at 125 °C: ○, and at 150 °C: ●. At densities above 0.1 g cm^{-3}, δ was fit as a linear function of density: m=1.97 cm^{-1}/(g cm^{-3}) and b=102.72 cm^{-1}.

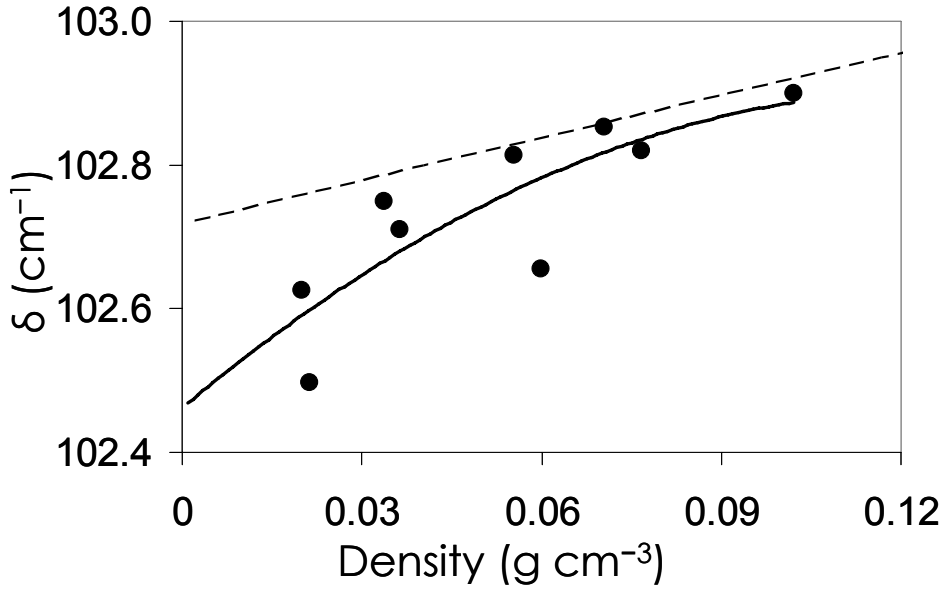

Figure 5B At densities below 0.1 g cm^{-3}, δ was fit as a second order polynomial with respect to density: a=−27.7523 $cm^{-1}/(g\ cm^{-3})^2$, b=7.004 $cm^{-1}/(g\ cm^{-3})$, and c=102.46 cm^{-1}. The dashed line represents an extrapolation of the linear calibration from A.

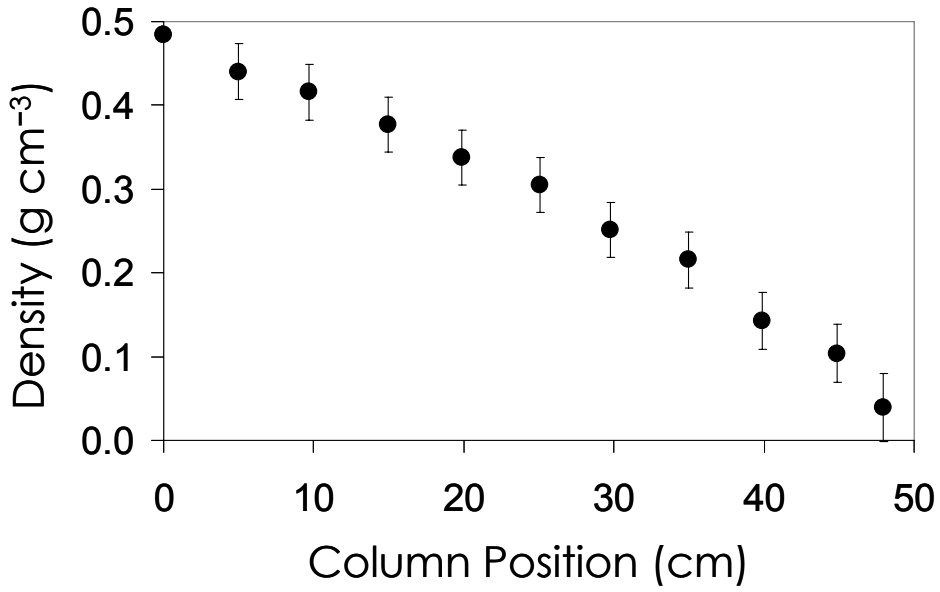

Figure 6 Density profile of an SGC column at 250 atm inlet pressure and 150 °C. The initial data point at 0 cm represents the calculated density based on the known temperature and inlet pressure. The error bars are 95% confidence intervals.

Conclusions

The frequency of the Fermi doublet in CO_2 is density dependent and has allowed me to observe the first experimental mobile phase density profiles in a packed capillary column. The relative intensity of the polarized bands in the Fermi doublet is also density dependent, but cannot be used to probe mobile phase density in packed columns due to the loss of polarization caused by column packing. I found that in attempting to calibrate fluid density to the absolute position of the Raman bands, spectral drift due to instrument instability was a significant source of error. This error can be eliminated by measuring the difference in frequency between the ν_1 and $2\nu_2$ bands even though it results in a less sensitive response factor. A more in-depth analysis of the flow behavior of compressible mobile phases and the effect of mobile phase compressibility on separation speed and efficiency based on the measured density profiles will be addressed in the following chapters.

References

[1] Y. Shen, M.L. Lee, Chromatographia 49 (1999) 333.

[2] S. Kuppers, M. Grosse-Ophoff, E. Klesper, J. Chromatogr. 629 (1993) 345.

[3] H. Janssen, H.M.J. Snijders, J.A. Rijks, C.A. Cramers, P.J. Schoenmakers, J. High Res. Chromatog. 14 (1991) 438.

[4] D.P. Poe, D.E. Martire, J. Chromatogr. 517 (1990) 3.

[5] P.E. Rothfusz, F. Verhoeven, P.J. Schoenmakers, J. Chromatogr. 395 (1987) 91.

[6] L.G.M. Uunk, P.J. Schoenmakers, Chromatographia 24 (1987) 51.

[7] Y.F. Shen, M.L. Lee, J. Chromatogr. 778 (1997) 31.

[8] R.L. Riester, T.J. Bruno, A. Hussam, D.P. Poe, D.E. Martire, J. Chromatogr. 545 (1991) 135.

[9] D.E. Martire, J. Chromatogr. 461 (1989) 165.

[10] G. Herzberg. Molecular Spectra and Molecular Structure. Van Nostrand, Princeton, 1945.

[11] G. Placzek. Mark Handbook der Radiologie. Akademishes Verlagsgesellshaft, Leipzig, 1934.

[12] R.B. Wright, C.H. Wang, J. Chem. Phys. 58 (1973) 2893.

[13] R.B. Wright, C.H. Wang, Chem. Phys. Lett. 23 (1973) 241.

[14] R.B. Wright, C.H. Wang, J. Chem. Phys. 61 (1974) 2707.

[15] Y. Garrabos, R. Tufeu, B. Le Neindre, G. Zalczer, D. Berysens, J. Chem. Phys. 72 (1980) 4637.

[16] Y. Garrabos, F. Echargui, F. Marsault-Herail, J. Chem. Phys. 91 (1989) 5869.

[17] Y. Garrabos, V. Chandrasekharan, M.A. Echargui, F. Marsault-Herail, Chem. Phys. Lett. 160 (1989) 250.

[18] G. Fanjoux, B. Lavorel, G. Millot, J. Raman Spectrosc. 29 (1998) 391.

[19] H. Nakayama, K. Saitow, M. Sakashita, K. Ishii, K. Nishikawa, Chem. Phys. Lett. 320 (2000) 323.

[20] H.L. Welsh, P.E. Pashler, B.P. Stoicheff, Can. J. Phys. 30 (1952) 99.

[21] A. Malik, W. Li, M.L. Lee, J. Microcolumn Sep. 5 (1993) 361.

[22] R.T. Jacobsen, R.J. Stewart, J. Phys. Chem. Ref. Data 2 (1973) 757.

Chapter 2: Density Gradients in Packed Columns with Compressible Mobile Phases Part I: Effects of Density Gradients on Analyte Retention and Separation Speed

Abstract

Density gradients in packed capillary columns operating over extreme pressure drops, typical for solvating gas chromatography, were investigated by on-column spectroscopic measurements and compared to a theoretical model. Laser-induced fluorescence was used to follow the elution of various analytes, and Raman spectroscopy was used to measure the density of the mobile phase, each with respect to column position. Mobile phase linear velocity initially increases gradually, and then rises rapidly near the column outlet. High flow rates near the column outlet are offset by a loss of mobile phase solvating power which ultimately limits the speed of supercritical fluid separations.

Introduction

Compressible mobile phases are used in a variety of chromatographic techniques, including gas chromatography (GC) and supercritical fluid chromatography (SFC). With compressible mobile phases, the pressure drop and corresponding expansion of the mobile phase gives rise to a density gradient along the column, which produces gradients in linear velocity, and in the case of SFC, solvating power of the mobile phase. These gradients in turn affect the retention time and the efficiency of a separation [1–5]. In open-tubular column separations, the column resistance factor is small, so pressure drop across the column is minimal. In packed columns, however, resistance to flow is greater, leading to large mobile phase density gradients.

To achieve low values of absolute plate height, small particles must be used. Several experiments have investigated the use of microparticles for packed column GC. Corcia et al. [6] reported a reduced plate height of 2.5 using 20-μm particles in a 21-cm long column. Lu et al. [7] packed a 10-cm long column with 7-μm particles and obtained a reduced plate height of 3.1. However, despite the high number of plates per unit length, the total column efficiencies in these experiments were relatively low. The total column efficiency can be increased by increasing the column length, but moderately long columns packed with microparticles have a high resistance to flow and require high column inlet pressures.

Shen and Lee [8] prepared a long (3 m) column packed with 10-μm particles. They operated this column at an inlet pressure of 260 atm. They reported a reduced plate height of 1.3 and a total column efficiency of 264 000. They also demonstrated that these separations were extremely fast relative to traditional methods. For these experiments, they used CO_2 as the carrier fluid; this allowed them to conveniently control the inlet pressure using an SFC pump. The carrier fluid was supercritical near the column inlet, which decreased retention due to the solvating power of supercritical CO_2 and allowed for faster elution of compounds that are too large for traditional GC. This technique is known as solvating gas chromatography (SGC) and can be thought of as a hybrid method between SFC and GC [8–10].

SGC provides a severe case for examining the effects of pressure drop on separation speed and efficiency. In SGC, the mobile phase is supercritical at the column inlet, but no flow restrictor is employed at the column outlet. The lack of a restrictor allows for high linear velocities of the mobile phase, but also results in large pressure

drops, leading to a loss of mobile phase solvating power and increasing analyte retention with respect to column position. The shape of the column density profile has been debated; Lee and coworkers [11] argued that the density should change linearly along the column. Others have challenged this idea, suggesting that the density change is more gradual until near the outlet of the column [12]. Theoretical studies [13–15] have not treated the large pressure drops that are found in SGC, and experiments aimed at direct measurement of mobile phase density or analyte retention with respect to column position have not been reported.

In this study, Raman spectroscopy and laser-induced fluorescence were used to measure the mobile phase density and observe analyte flow directly on-column. The measured mobile phase density profiles are compared to a theoretical model which provides understanding about the flow behavior of compressible mobile phases in packed capillaries. Comparison of the mobile phase flow with analyte elution profiles provides a better understanding of the effects of fluid compressibility on the speed of supercritical fluid separations.

Experimental

Laser-induced Fluorescence Experiments

Several polycyclic aromatic hydrocarbons were monitored as they eluted through the column by monitoring laser-induced fluorescence as a function of time after injection at a number of points along the column (see Figure 1). Benzene, naphthalene, and phenanthrene were chosen because they range from weakly to highly retained, and they can all be monitored by laser-induced fluorescence.

The frequency-doubled output of an excimer-pumped dye laser (LPX 200/Scanmate, Lambda Physik) at 255 nm was used to excite all of these compounds. The incident angle between the excitation laser beam and the capillary was approximately 45°. A UV-enhanced aluminum mirror was used to fold the scattered emission toward the entrance slit of a 1/3-m monochromator (Instruments SA, Metuchen, NJ). A lens focused the emission onto the entrance slit of the monochromator with 1:1 imaging, and a long-pass 295-nm cutoff filter helped to block scattered excitation light from the excitation source. Emission from benzene, naphthalene, and phenanthrene was monitored at 292 nm, 334 nm, and 368 nm, respectively. A photomultiplier tube (Bialkali, Thorn EMI, Fairfield, NJ) was used to detect the fluorescence, and a boxcar integrator (PAR 162, EG&G, Princeton, NJ) processed the signal. The time constant and aperture of the integrator and the repetition rate of the laser were adjusted to minimize distortion of the time-dependent signal. A LabVIEW (Austin, TX) program recorded the data from the integrator. The top of the peak was used as a measurement of retention time. Retention times reported in this paper are an average of 3–9 injections.

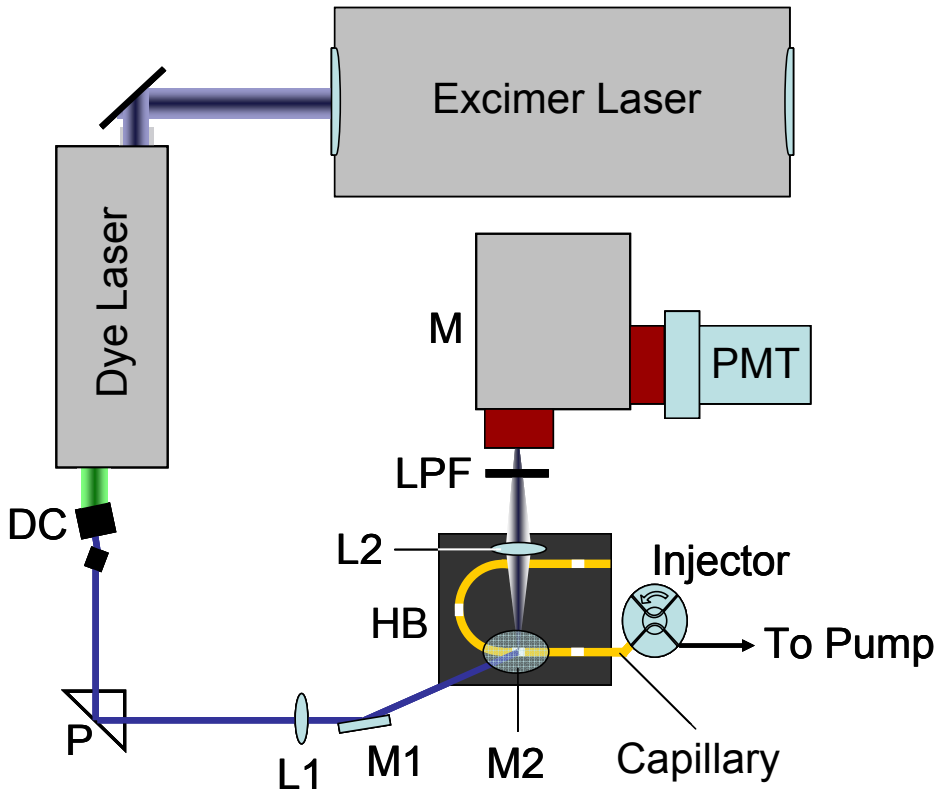

Figure 1 Experimental setup for on-column detection of fluorescent analyte. DC: doubling crystal; P: prism; L1 and L2: lenses; M1 and M2: mirrors; LPF: long pass filter; HB: heating block; M: monochromator; PMT: photomultiplier tube.

Materials

Porous (100 Å), spherical octadecyl bonded silica (ODS) particles with 5 μm diameters were purchased from Macherey-Nagel (Duren, Germany). Fused silica capillary tubing (250 μm i.d./365 μm o.d.) was purchased from Polymicro Technologies (Phoenix, AZ). Column connections were made with PEEK tubing (Upchurch Scientific, Oak Harbor, WA) and zero dead-volume unions (Valco Instruments, Houston, TX). Reagent grade CO_2 was used for the preparation of packed capillary columns. SFC grade CO_2 (Scott Specialty Gases, Plumsteadville, PA) was used as the mobile phase. Coumarin 503 laser dye was purchased from Lambda Physik (Fort Lauderdale, FL).

Preparation of Columns

A CO_2 slurry packing method was used to prepare the packed capillary columns [16]. Columns were approximately 52 cm in length. A 2-μm steel screen (Valco) was positioned at the end of the column, inside a zero-dead-volume union to support the particles. Particles were packed into the column with CO_2 at 60 atm, and then the pressure was slowly increased to 300 atm. During packing, the column was placed in an ultrasonicator to help settle the particles. The column was conditioned in the ultrasonicator by holding the pressure at 300 atm for 10 min. Finally, the column was slowly depressurized over a period of several hours. Marisa measured the total column porosity by the gravimetric method described by Berendsen et al. [17]. The total column porosity was found to be 0.7.

Windows, 3–5 mm wide, were placed along the column about every 2–4 cm to allow for optical detection of the solutes. The windows were made by stripping the polyimide coating from the outer capillary wall with hot sulfuric acid. Fragility of the

bare fused silica capillary limited the minimum spacing between the windows. Even so, with the polyimide coating removed from the window sections, the columns were fragile enough, especially under pressure, that they often shattered before a complete set of measurements could be made, and so the results reported here represent a compilation of data from multiple columns.

Temperature Control

To maintain the capillary column at a constant temperature while allowing on-line optical detection, the capillary was placed on an aluminum heating block. The block was 0.75 inch thick and 5 × 11 inches in width and length. On one face, a groove was milled 0.020 inches wide and deep to accommodate the capillary. At each end of the groove, wells were milled to house the dead volume unions connected to the capillary column. Plates of fused silica and glass placed on top of the aluminum block held the capillary in place and insulated it, while allowing for optical detection. The block was heated by a heating plate. To test for temperature evenness, a thin thermocouple was threaded down the capillary groove and the temperature recorded at various points. At 62.5 °C, the temperature along the capillary groove varied by less than ± 0.2 °C. At 179.0 °C, the temperature along the capillary groove varied by less than ± 1.4 °C.

SGC Setup

Pressure of the CO2 mobile phase was controlled by a Varian Model 8500 SFC pump (Walnut Creek, CA) and monitored by a grade 3A Ashcroft test gauge, calibrated to 0.25%. Samples were introduced onto the column with a Valco pneumatic injector having a rotor volume of 0.2 μL. No flow restrictor was employed at the end of the column, other than the retaining screen for the packing material. Factors such as dead

volume, particle size, split-ratio, and temperature were not optimized for the solute components used in this study. Although not optimized for analytical separations, the chromatographic set-up in this study adequately served the purposes of this study.

Density Measurements

The density of the CO_2 mobile phase in an SGC column was measured directly on-column by Raman spectroscopy. The details of these measurements are described in reference [18]. In short, the frequency of the Fermi doublet in CO_2 is density dependent and allows for the determination of mobile phase density. Making these measurements at varying positions along the column yielded the mobile phase density profile. The column packing and operating parameters for the Raman density measurements were similar to those described above for the fluorescence measurements and are reported in detail in reference [18]. Density profiles were measured for an SGC column operating at 125 and 150 °C for inlet pressures of 160, 220, and 280 atm. Again, results represent the compilation of data from multiple columns, due to the fragile nature of the column when the polyimide coating is removed to form the windows.

Performance of Calculations

Calculations were performed with MathCad, using several in-house routines. The theory is described below, but calculations required a number of inputs. Mobile phase flow rate was measured with a bubble flow meter. Density values for CO_2 were obtained from the Jacobsen-Stewart modification of the Benedict-Webb-Rubin (BWR) [19] equation of state

$$P = \rho RT + \sum_{i=1}^{32} N_i X_i \qquad (1)$$

where values for N_i and X_i were obtained from Martire et al. [14]. Because this equation is a complicated function of density, the root function in Mathcad was used to solve for density at the various pressures. Viscosities were obtained from the equation of Stephan and Lucas [20]

$$\eta_R = \sum_{i=0}^{4}\sum_{j=0}^{4} c_{i,j} T_R^j \rho_R^i \qquad (2)$$

where $\rho_R = \rho/\rho_c$, $T_R = T/T_c$, $\eta_R = \eta/\eta^o$, and η^o is the viscosity at one bar for a given temperature. The $c_{i,j}$ coefficients for CO_2 were obtained from Martire et al. [13].

Results and Discussion

Analyte Retention Profiles

Figure 2 shows the retention time profile for benzene at a temperature of 180 °C and inlet pressures of 250, 175, and 140 atm. Because the data are plotted as time for a solute band to reach each window (i.e., migration time vs distance along the column), a constant slope means a constant rate of elution; a decreasing slope, an increasing rate of elution; and an increasing slope, a decreasing rate of elution. To aid rapid comprehension of the results, accompanying the retention time profiles are elution rate profiles, calculated from the derivative of a polynomial fit to the retention time profiles. At 250 atm, the velocity of benzene is nearly constant up to about the mid-point on the column. At this point on the column, elution rate begins to increase. Because at 180 °C benzene is weakly retained [6], its behavior is expected to closely follow the flow behavior of the mobile phase, although the slight retention of benzene causes its elution profile to vary somewhat from the mobile phase linear velocity profile. At the lower head pressures, similar behavior is observed, but with increasing retention time and steeper curvature in

the retention profiles as the solvating power of the mobile phase decreases and retention of benzene becomes stronger.

Figure 3 shows retention time profiles of benzene at 100 °C and 130 °C at an inlet pressure of 250 atm. At these lower temperatures, the retention of benzene becomes more dependent on the solvating power of the mobile phase, and an increase in the retention of benzene competes with increasing flow rate as mobile phase density drops along the column. The retention time profile at 100 °C indicates that the mobile phase loses solvating power well before the mid-point of the column. Near the column inlet, retention is weaker because density is greater and the mobile phase is more solvating. Retention increases toward the end of the column because the density is lower and the mobile phase is less solvating. At 130 °C, the increasing flow rate, caused by expansion of the mobile phase, appears to exactly counter-balance the increase in retention. At higher temperatures and an inlet pressure of 250 atm (Figure 2), the profile is dependent primarily on mobile phase linear velocity. Of course, changes in temperature also affect the density of the mobile phase. A temperature change from 100 °C to 180 °C can change the mobile phase density by 40%. However, a change in viscosity of the mobile phase acts to counter the effect of density on the mobile phase linear velocity.

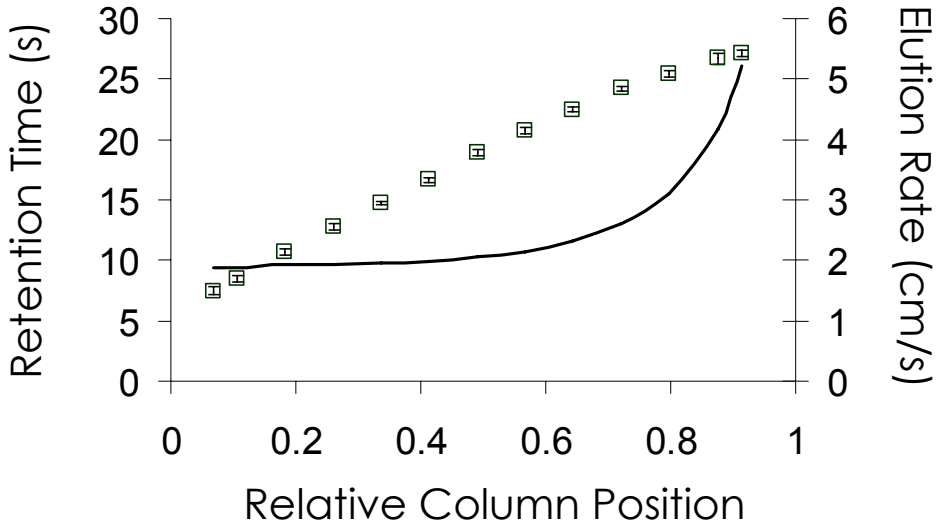

Figure 2A Retention time profile (□) and linear velocity profile (—) of benzene at 180°C and 250 atm inlet pressure.

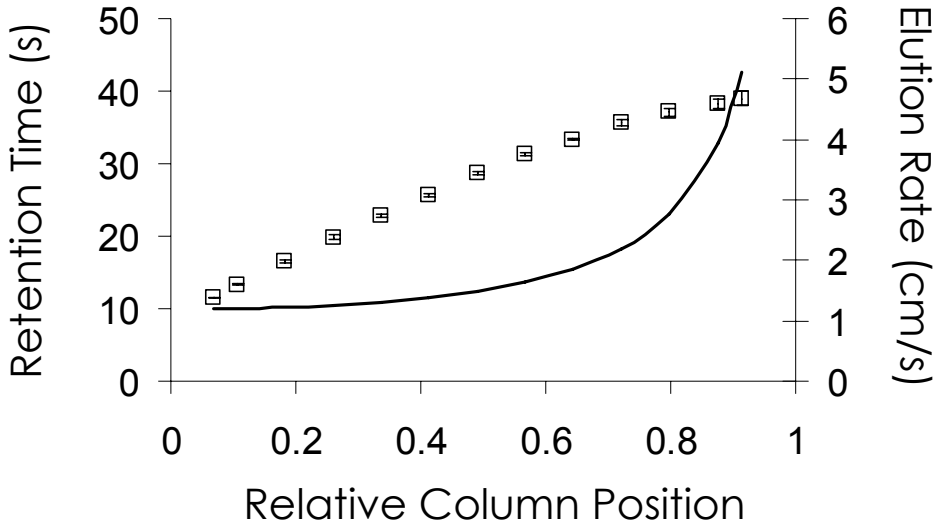

Figure 2B Retention time profile (□) and linear velocity profile (—) of benzene at 180°C and 175 atm inlet pressure.

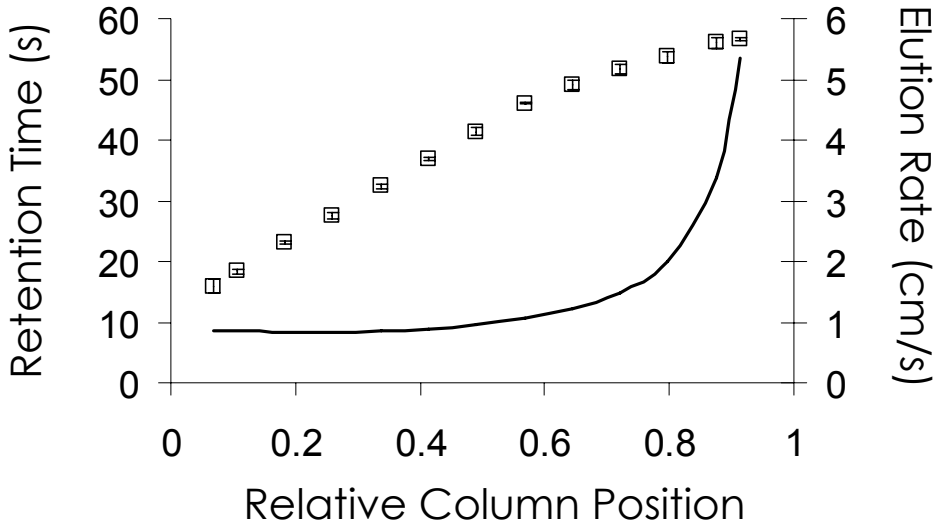

Figure 2C Retention time profile (□) and linear velocity profile (—) of benzene at 180°C and 140 atm inlet pressure.

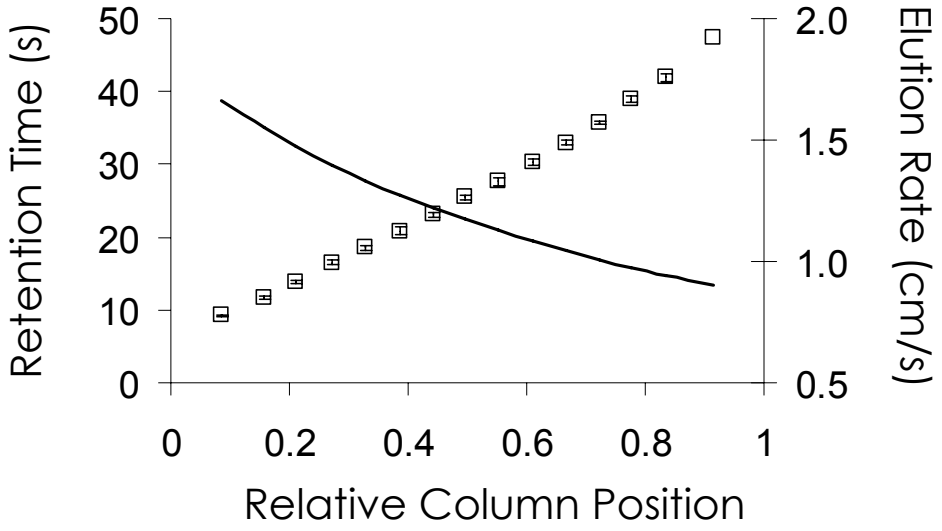

Figure 3A Retention time profile (□) and linear velocity profile (—) of benzene at 100 °C and 250 atm inlet pressure.

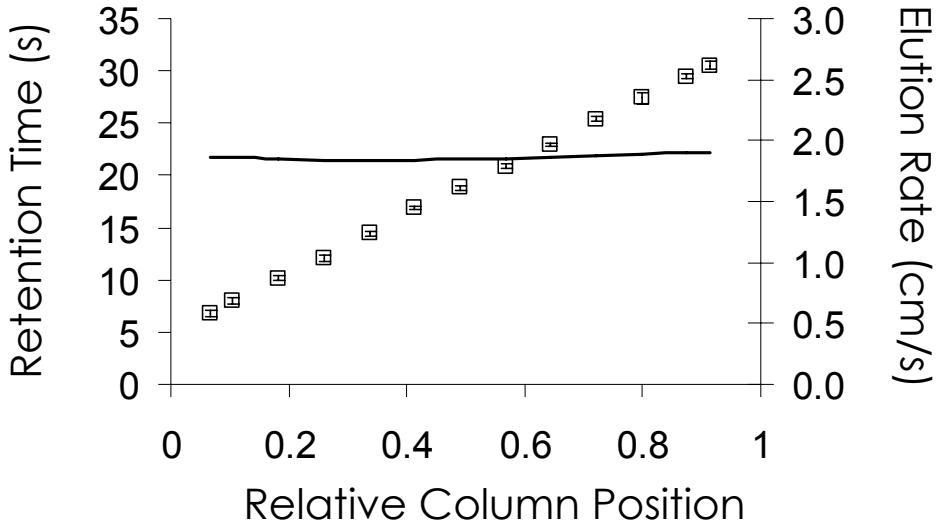

Figure 3B Retention time profile (□) and linear velocity profile (—) of benzene at 130 °C and 250 atm inlet pressure.

Figure 4 shows the retention time profiles of phenanthrene at inlet pressures of 140, 175, and 250 atm at 180°C. These profiles of phenanthrene show a step in retention at about mid-point of the column. These shifts in the retention time profiles of phenanthrene indicate a transition to more GC-like conditions, where the mobile phase is much less solvating. At higher inlet pressures, the step in the retention profiles shifts closer to the column outlet. Therefore, in terms of solvating properties and retention characteristics, the separation behaves more like SFC at higher inlet pressures. At 250 atm, the elution rate of phenanthrene continually decreases over the length of the column. However, at 140 and 175 atm, the elution rate increases as phenanthrene nears the end of the column. The increase in the elution rate of phenanthrene near the end of the column at 140 and 175 atm shows that, at a temperature of 180 °C, the mobile phase linear velocity has a great influence on the elution rate of phenanthrene despite strong retention caused by a loss of mobile phase solvating power.

Figure 5 shows the retention time profile of phenanthrene at 100°C and an inlet pressure of 250 atm, revealing the pronounced effects of increasing retention with the loss of mobile phase density. At the beginning of the column, the elution rate of phenanthrene slightly decreases. At about three-tenths of the column length, the elution rate profile changes dramatically because the retention of phenanthrene is more strongly dependent on mobile phase density than is retention of benzene, especially at low temperature.

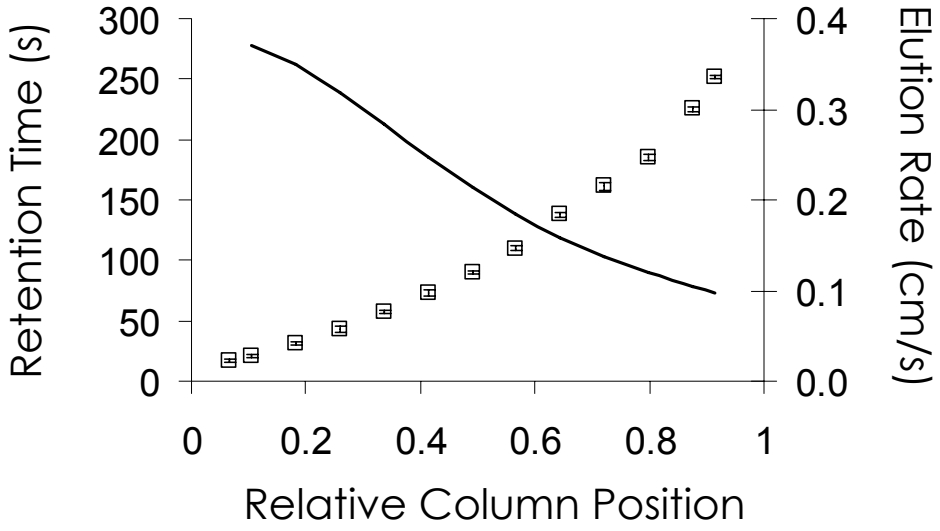

Figure 4A Retention time profile (□) and linear velocity profile (—) of phenanthrene at 180°C and 250 atm inlet pressure.

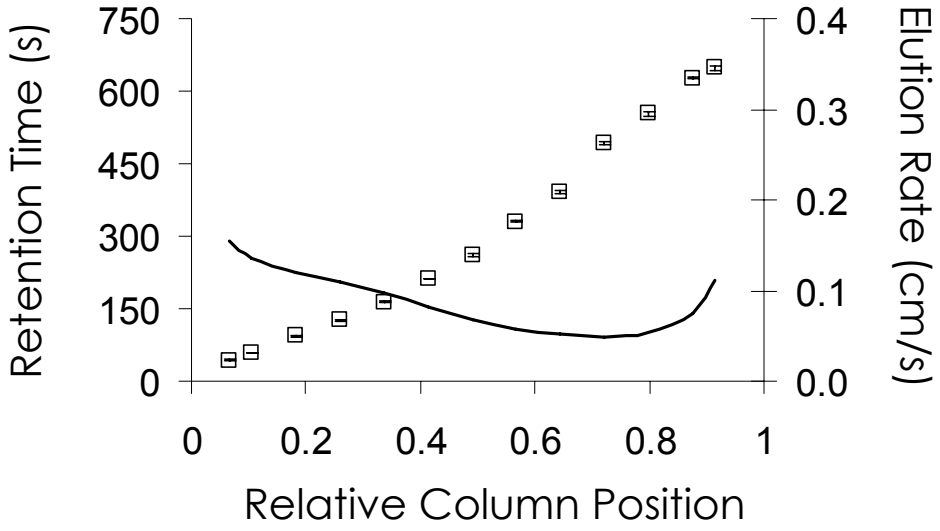

Figure 4B Retention time profile (□) and linear velocity profile (—) of phenanthrene at 180°C and 175 atm inlet pressure.

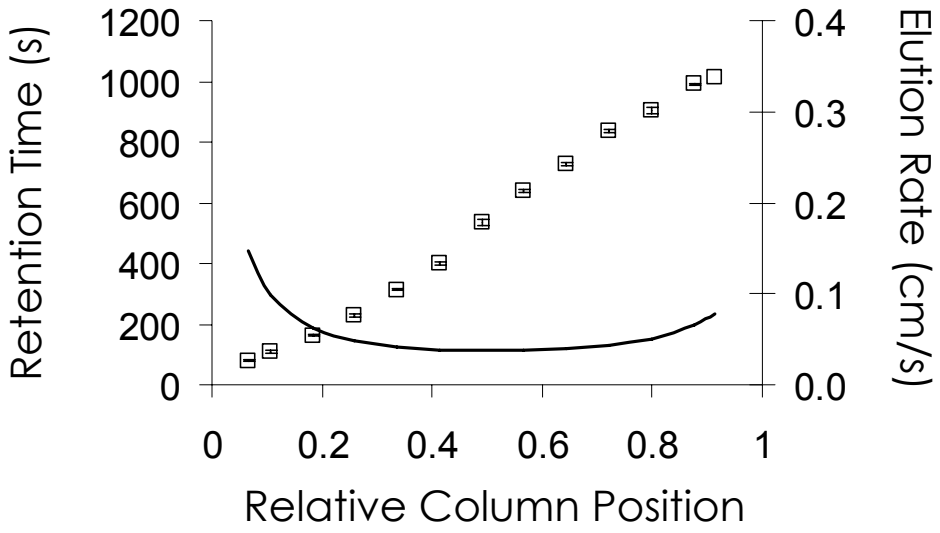

Figure 4C Retention time profile (□) and linear velocity profile (—) of phenanthrene at 180°C and 140 atm inlet pressure.

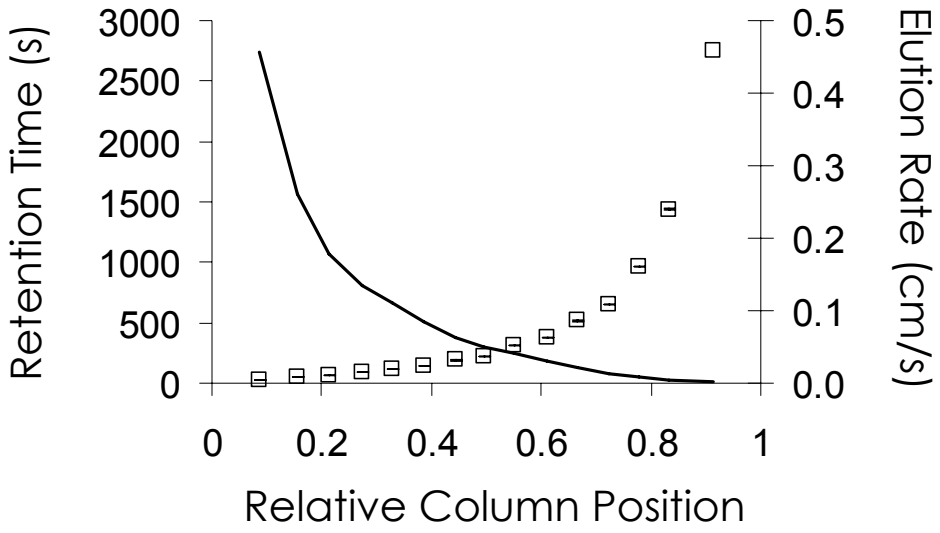

Figure 5 Retention time profile (□) and linear velocity profile (—) of phenanthrene at 100 °C and 250 atm inlet pressure.

Measurements were also made for naphthalene and pyrene. The results for naphthalene are intermediate to those shown for benzene and phenanthrene. Pyrene continues the trend to even stronger curvature in the retention time profiles, and in fact, beyond mid-column, its retention times became impractically long.

Mobile Phase Flow Profiles

A more complete understanding of the elution rate of the various compounds requires an understanding of the linear velocity profile and the actual density of the mobile phase. Raman spectroscopy allowed measurement of the mobile phase density profile along the column (as described in reference [18]), and from that the linear velocity profile could be determined by mass balance. Figure 6 shows the measured mobile phase density gradients for columns at 160 and 280 atm inlet pressure. Density gradients were also measured at 220 atm, but for purposes of reducing congestion in the figure, they have been left out; the other profiles show the same overall behavior but intermediate to the two shown. The error bars shown represent 95% confidence intervals, and the data points at 0 cm, or the column inlet, are the known column inlet densities determined from the column head pressure. These profiles show that density changes fairly gradually over the first half of the column, but the gradient becomes increasingly steep near the column outlet. This qualitatively agrees with the elution profiles of benzene at high temperatures, which showed a nearly constant elution rate for the first half of the column and then an accelerating rate of elution nearing the column outlet.

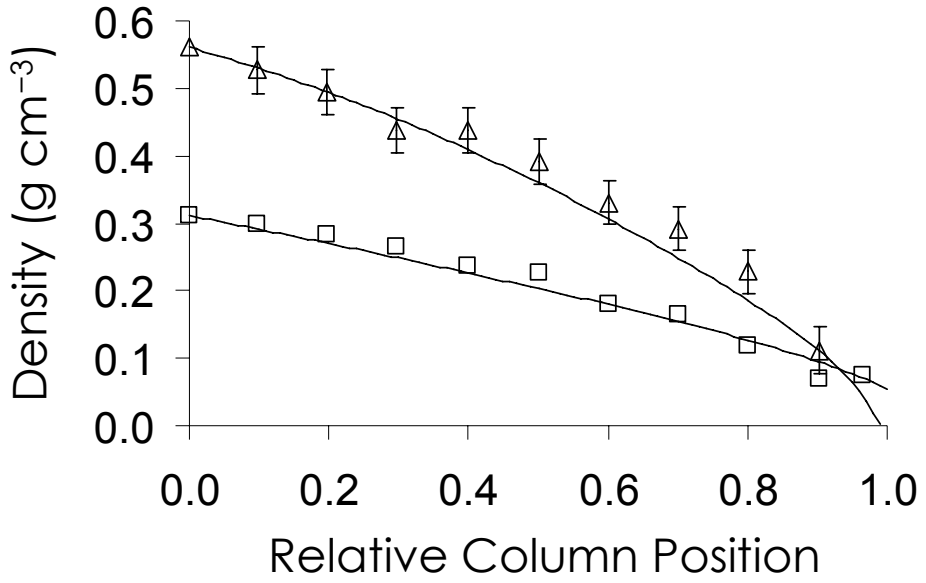

Figure 6A Density profiles of an SGC column at 125 °C. □ represent direct measurements of CO_2 density for 160 atm inlet pressure, and △ represent density measurements for 280 atm inlet pressure. The error bars give 95% confidence intervals for the measured densities. The solid lines show the theoretical column density profiles calculated by applying the Darcy equation in a stepwise manner across short column segments.

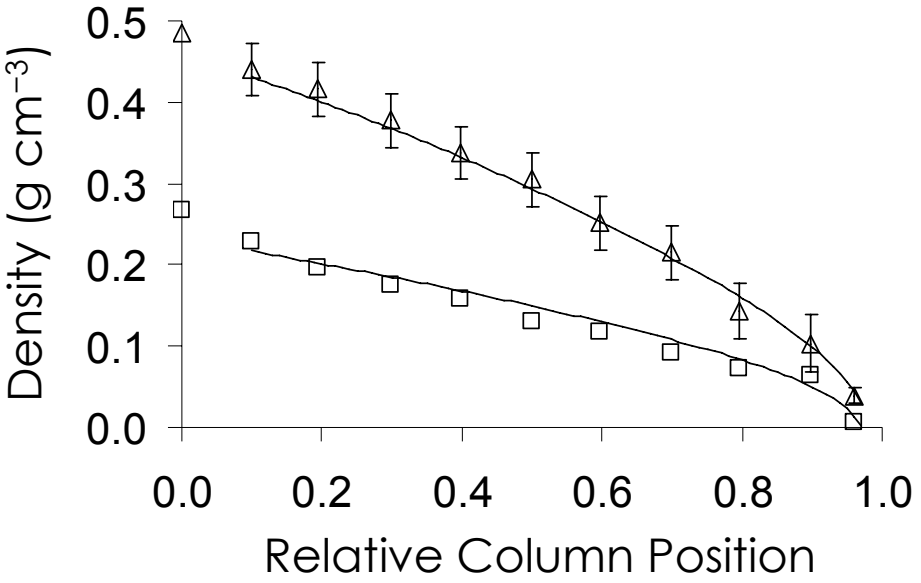

Figure 6B Density profiles of an SGC column at 150 °C. □ represent direct measurements of CO_2 density for 160 atm inlet pressure, and △ represent density measurements for 280 atm inlet pressure. The error bars give 95% confidence intervals for the measured densities. The solid lines show the theoretical column density profiles calculated by applying the Darcy equation in a stepwise manner across short column segments.

To model these density profiles theoretically, I followed the approach described by Martire et al. [13, 14]. They started with Darcy's law and derived general equations for the spatial and temporal density distribution functions. Although Darcy's equation applies strictly to incompressible fluids, it can be adapted to compressible fluids by applying it over short segments in a stepwise manner. The Darcy equation is

$$\Delta P = B_0 \cdot \eta \cdot u_0 \cdot L \tag{3}$$

where ΔP is pressure drop across the column, η is the fluid viscosity, L is the length of the column, u_0 is the superficial mobile phase velocity or the mobile phase velocity assuming a tube with no packing, and B_0 is the permeability coefficient of the column. For packed columns

$$B_0 = \frac{\varphi_0}{d_p^2} \tag{4}$$

where φ_0 is the column resistance factor, and d_p is the particle diameter.

The superficial linear velocity can be calculated from

$$u_0 = \frac{4m_f}{\pi \cdot \rho \cdot d_c^2} \tag{5}$$

where m_f is the mass flow rate of the column, d_c is the diameter of the empty column, and ρ is the density of the fluid. Substitution of equation (3) into equation (1) yields

$$\Delta P = \frac{4B_0 \cdot \eta \cdot m_f \cdot L}{\pi \cdot \rho \cdot d_c^2} \tag{6}$$

For compressible fluids, the column is divided into n short segments of equal length, dL, and the pressure drop is calculated for each segment i along the column. For the model calculations, the segment length, dL, was set to 0.5 cm. I used empirically determined mass flow rates for the columms. All other parameters except for the column

resistance factor, φ_0, were known or could be calculated as described in the Experimental section, but φ_0 could not be independently measured. It is therefore the single adjustable parameter used in fitting the model to my data.

Solving these equations iteratively for each column segment produced theoretical mobile phase density profiles which are shown as the fits to the measured density in Figure 6. As can be seen, the model closely agrees with the measured densities for the runs at 125 °C. The runs at 150 °C show a slight drop in density between the column inlet and the first data point, suggesting a mild pressure drop in the connecting union. However, if density is modeled starting from the first measured data point, these runs also show close agreement to the model. The value of the column resistance factor varied between 1250 and 1325 for one column and was 1550 for a second column, which are reasonable values.

Column fittings prevented me from making measurements any closer to the end of the column than a few millimeters, but the model calculations have no such limitation. Knowledge of the column density gradient allows calculation of the elution rate of an unretained compound for comparison to the observed analyte retention profiles. Assuming the compound is fully penetrating, the elution rate, u_m, is given by

$$u_m = \frac{4m_f}{\pi \cdot d_c^2 \cdot \rho \cdot \varepsilon_t} \qquad (7)$$

where ρ is the mobile phase density, and ε_t is the total column porosity. As described above, the total column porosity was 0.7. From this I calculated elution profiles for an unretained component in an SGC column operating at 250, 175, and 140 atm inlet pressures and 130 °C. These elution profiles are shown in Figure 7.

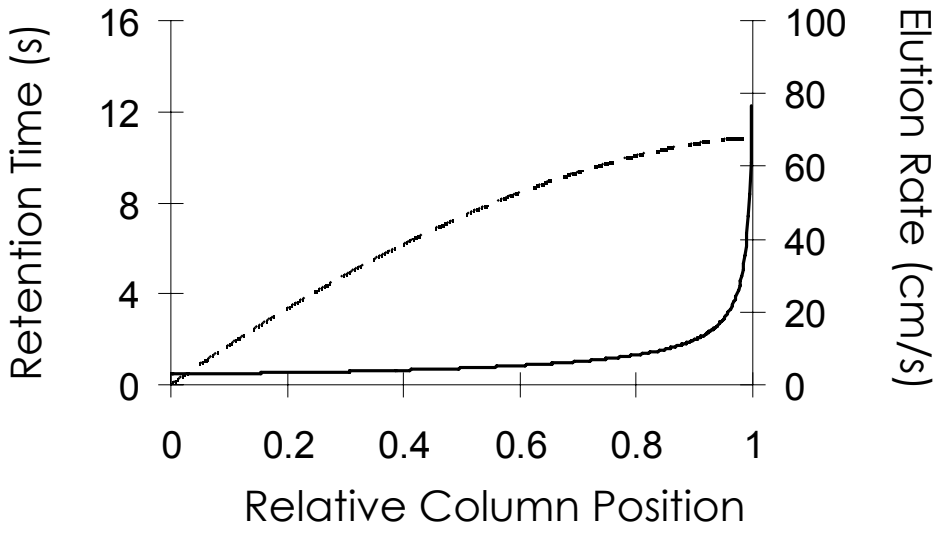

Figure 7A Retention time profile (– –) and linear velocity profile (—) of an unretained component at 130°C and 250 atm inlet pressure.

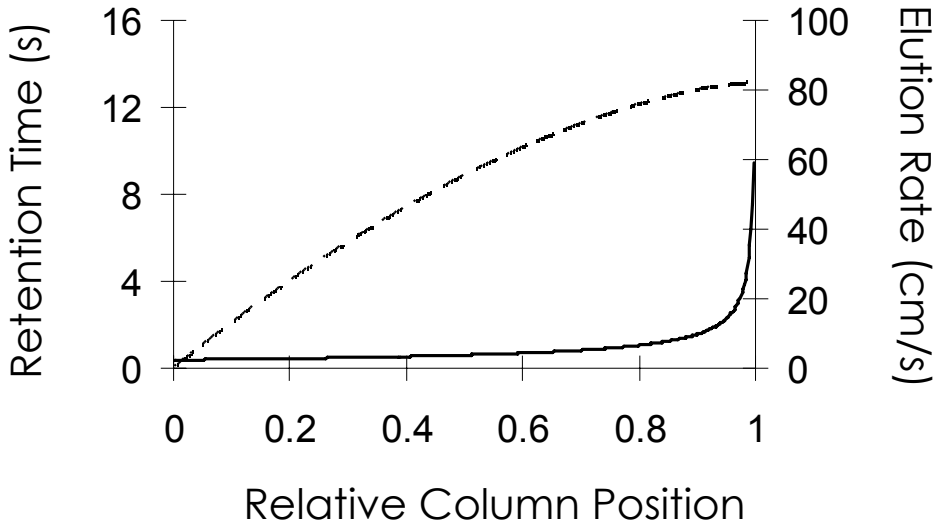

Figure 7B Retention time profile (– –) and linear velocity profile (—) of an unretained component at 130°C and 175 atm inlet pressure.

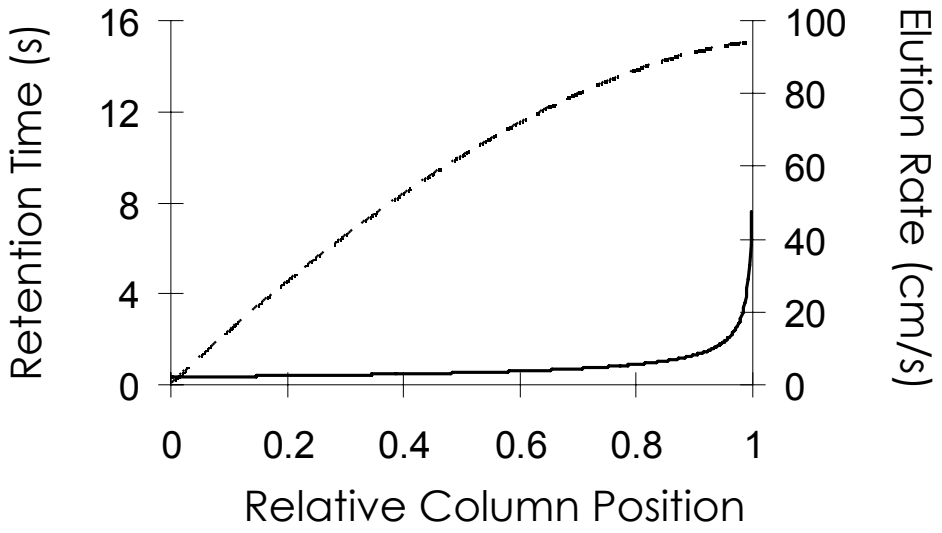

Figure 7C Retention time profile (– –) and linear velocity profile (—) of an unretained component at 130°C and 140 atm inlet pressure.

Conclusions

Combining observations of analyte elution and mobile phase flow profiles reveals the factors that control separations in packed columns when compressible fluids are employed. For small, weakly retained compounds, the shape of the elution profiles closely parallels the flow behavior of the mobile phase. In the case of larger compounds, the elution profiles show the combined effects of increasing mobile phase velocity and increasing analyte retention with column pressure drop. Density gradients result in increased flow rates near the column outlet, and the rate of increase becomes increasingly steep with respect to column position. However, the effect of increasing mobile phase linear velocity is offset by increased retention as the solvating power of the mobile phase decreases with decreasing density. As a result, elution in SGC is consistent with SFC-like conditions for about the first half of the column and then becomes more like a GC separation. It is important to note, however, that in these experiments, although pressures became subcritical, temperature did not, so no phase transition occurred.

The density profile of a compressible mobile phase in a packed capillary can be modeled by applying the Darcy equation for pressure drop in a step-wise manner over short column segments. Direct measurement of mobile phase density shows this model to be accurate for columns operating across pressure drops up to 280 atm. This model provides a clear description of mobile phase flow behavior in packed capillaries. At high flow rates, the density gradient is approximately linear over the first half of the column and becomes increasingly steep near the column outlet where mobile phase velocity becomes high, approaching 100 cm/s for typical SGC conditions, assuming that the model can be accurately extrapolated to the end of the column.

At first appearance, efficiency seems to become rapidly worse as retention increases while mobile phase linear velocity increases. However, this is not the case, as is considered in detail in the following paper. The limiting factor for separations with SGC, then, is not efficiency, but excessively long elution times for less volatile compounds. Large retention gradients exist at low temperatures with large molecules. However, increasing the column temperature decreases analyte retention and can compensate for increased retention in the low density region of the column. These results suggest that a temperature gradient applied along the length of the column can offset this limitation, and experiments are currently underway to test this hypothesis.

References

[1] S.M. Fields, M.L. Lee, J. Chromatogr. 349 (1885) 305.

[2] P.J. Schoenmakers, F.C.J.G. Verhoeven, J. Chromatogr. 352 (1986) 315.

[3] K.D. Bartle, T. Boddington, A.A. Clifford, G.F. Shilstone, J. Chromatogr. 471 (1989) 347.

[4] P.J. Shoenmakers, L.G.M. Uunk, Chromatographia, 24 (1987) 51.

[5] P.A. Mourier, M.H. Caude, R.H. Rosset, Chromatographia, 23 (1987) 21.

[6] A. DiCorcia, A. Liberti, R. Samperi, J. Chromatogr. 167 (1978) 243.

[7] C.P. Lu, LM. Zhou, C.H. Wang, G.G. Wang, A.Z. Xia, F.B. Xu, J. Chromatogr. 1979 (186) 20.

[8] Y. Shen, M.L. Lee, Anal. Chem. 69 (1997) 2541.

[9] Y. Shen, M.L. Lee, Chromatographia 46 (1997) 537.

[10] Y. Shen, M.L. Lee, J. Chromatogr. 778 (1997) 31.

[11] M.L. Lee, Presented in Chem 629 lecture, Provo, UT, 2000.

[12] Personal communication, T. Chester, 2000.

[13] D.E. Martire, J. Chromatogr. 461 (1989) 165.

[14] R.L. Riester, T.J. Bruno, A. Hussam, D.P. Poe, D.E. Martire, J. Chromatogr. 545 (1991) 135.

[15] H.G. Janssen, H.M.J. Snijders, J.A. Rijks, C.A. Cramers, P.J. Schoenmakers, J. High Resolut. Chromatogr. 14 (1991) 438.

[16] A. Malik, W. Li, M.L. Lee, J. Microcolumn Sep. 5 (1993) 361.

[17] G.E. Berendsen, P.J. Schoenmakers, L. De Galan, G. Vigh, Z. Varga-Puchony, J. Inczedy, J. Liq. Chromatogr. 3 (1981) 13.

[18] Submitted for publication, Appl. Spectrosc.

[19] R.T. Jacobsen, R.J. Stewart, J. Phys. Chem. Ref. Data, 2 (1973) 757.

[20] K. Stephan, K. Lucas, Viscosity of Dense Fluids. Plenum Press, New York, 1979.

Chapter 3: Density Gradients in Packed Columns with Compressible Mobile Phases Part II: Effects of Density Gradients on Separation Efficiency

Abstract

On-column detection provided a direct measure of band dispersion along a packed capillary operating under solvating gas chromatography (SGC) conditions, and efficiency was calculated with respect to column position. Theoretical efficiency of an SGC column was modeled for comparison to on-column measurements. The model indicates that the primary cause of band broadening in SGC is high mobile phase velocity near the column outlet. The experimental results show that additional band broadening can be correlated to high analyte velocities. On-column detection also showed spatial focusing of the analyte as it moves down the column density gradient.

Introduction

To achieve fast, high efficiency separations, fast diffusion of analyte in the mobile phase and a small critical diameter of the column are needed. Gases and supercritical fluids are commonly used as the mobile phase for chemical separations because they allow for fast analyte diffusion and have low viscosity relative to liquids. In the case of packed column separations, where a small particle diameter improves efficiency, high column inlet pressures are often needed to generate flow. Consequently, high efficiency chromatography is often characterized by a compressible mobile phase flowing down a large pressure gradient. This results in on-column expansion of the mobile phase and leads to a gradient separation where local efficiency can vary as a function of column

position. Much work has been done to understand the effect of column pressure drop on compressible mobile phase separations.

In gas chromatography (GC), column pressure drop results in expansion of the carrier fluid near the column outlet leading to an increase in mobile phase velocity. Theoretical work by Giddings [1] suggests that even severe pressure drops in GC will not adversely affect column efficiency. To test this conclusion, Meyers and Giddings [2] prepared a 4000 ft column packed with 50–60 mesh particles. Operating this column at 2500 psi inlet pressure, they obtained a reduced plate height of 2. This is the lowest reduced plate height ever reported in packed-column GC.

Unlike in GC, the mobile phase in supercritical fluid separations can reduce retention by solvating the analyte. Because the solvating power of a supercritical fluid is a strong function of density, column pressure drops lead to gradients in analyte retention factors as well as mobile phase velocity. Consequently, determining the effect of pressure drop on column efficiency is more complicated for supercritical fluid chromatography (SFC) and solvating gas chromatography (SGC) than for GC.

A number of studies have looked at the effect of pressure drop on efficiency in SFC [3–7]. Schoenmakers and Uunk [6] showed that pressure drop had a minimal effect as long as the minimum column density was kept above a threshold value. However, if the column outlet density was allowed to drop too low, then decreased column efficiency was observed. Mourier et al. [7] reported band broadening with increased pressure drop and observed that band broadening was greatest at low column inlet pressures. Other investigators [8–10] have found no loss of efficiency with pressure drop for typical SFC conditions. However, in these experiments, the authors treated analyte retention factors,

diffusion coefficients, and mobile phase velocity in terms of column averages. These approximations are not valid under conditions of high mobile phase compressibility or large pressure drops when local conditions can differ significantly from column averages.

Martire and Poe [11] derived expressions for observed plate height based on theoretical column density gradients. Using these equations, they looked at the effects of column pressure drop on efficiency in open tubular SFC. These calculations supported the qualitative observations of Shoenmakers and Uunk [6] and Mourier et al. [7]. However, this work did not attempt to address the larger pressure drops observed in packed column SFC or in SGC due to the complexity of calculating these density gradients. Janssen et al. [12] theoretically modeled density gradients for columns operating across a large pressure drop by applying the Darcy equation in a stepwise manner over short column segments. Applying this model to open tubular SFC allowed them to use the equations presented by Martire and Poe [11] to calculate the efficiency of open-tubular columns operating over pressure drops as high as 60 bar. Comparison of the model with experimental efficiency measurements yielded good agreement except at high pressure drops, where observed efficiency was greater than the model predicted. However, they did not model the efficiency of packed columns because unknown empirical coefficients made plate height calculations difficult.

The effect of column gradients on separation efficiency has been difficult to study because traditional detection only yields information on the average effect of local column conditions. In this work, on-column detection provides a measure of band dispersion with respect to column position and allows for observed efficiency to be correlated to local column conditions. Additionally, knowledge of mobile phase flow

allows for efficiency modeling of an SGC column for comparison to experimental measurements. This work provides a more complete understanding of the effects of pressure drop on the efficiency of compressible mobile phase separations in packed columns.

Experimental

Band dispersion was measured with respect to column position using laser-induced fluorescence. The experimental setup, column preparation, and operating conditions were identical to those described in the previous chapter. Peak widths were measured for naphthalene and phenanthrene at 140, 175, and 250 atm inlet pressure. The column temperature for these runs was 130 °C. Peak widths reported in this paper are an average of 3 injections.

Results and Discussion

Efficiency

It is important to distinguish between apparent plate height and local plate height. When detecting at the column outlet, apparent plate height describes the average efficiency of the entire column. However, even when detecting on column, the observed plate height does not directly yield a measure of local efficiency, because the observed efficiency still represents an average for the portion of the column preceding the point of detection. To determine actual values for local efficiency, it is necessary to divide the column into segments and consider the contribution to dispersion in each individual segment.

The apparent plate height, $\hat{H}$, is defined as

$$\hat{H} = \frac{L \cdot \tau^2}{t^2} \qquad (1)$$

where L is the distance the analyte has traveled, τ is the temporal band dispersion, and t is the elapsed time [11]. If the column is divided into segments of length dL, the local plate height, H_i, of each segment is given by

$$H_i = \frac{dL \cdot \tau_i^2}{t_{R,i}^2} \quad (2)$$

where τ_i is the contribution to dispersion in segment i, and $t_{R,i}$ is the residence time of the analyte in that segment [11]. It is important to note that τ and t_R sum differently: $\tau^2 = \Sigma\tau_i^2$, while $t_R = \Sigma t_{R,i}$ [13]. This relationship allows me to calculate the contribution to band dispersion in each column segment and determine values for local plate height.

Figure 1 shows the observed band dispersion, τ, for naphthalene and phenanthrene as a function of column position. To calculate the local efficiency from these plots, I fit each dispersion profile to a polynomial and determined τ_i with respect to column position, where each segment i was the distance between observations. Then I calculated the corresponding $t_{R,i}$ from fits of the retention profiles. The length, dL, was taken as the distance between on-column observations. Using τ_i, $t_{R,i}$, and dL, I calculated local plate height as a function of column position using equation (2).

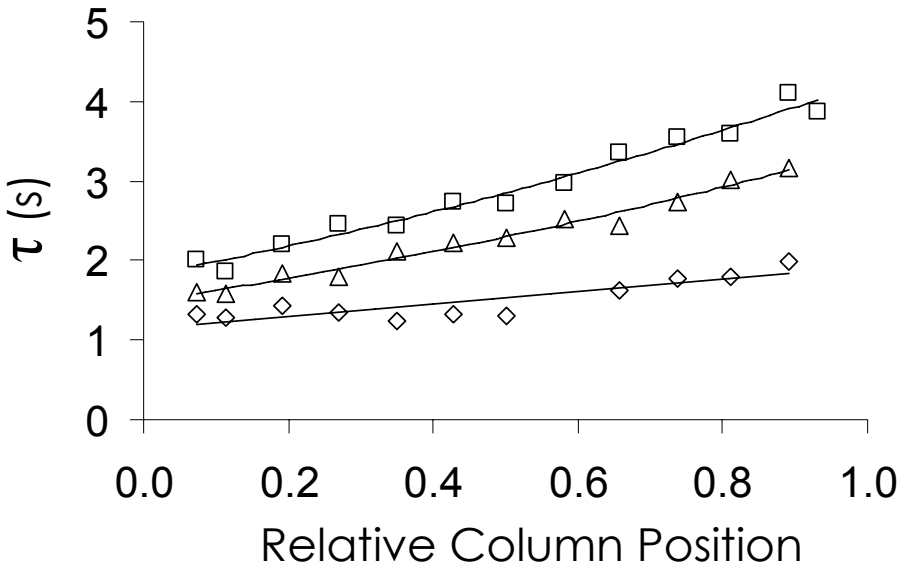

Figure 1A Temporal band dispersion profiles of naphthalene in an SGC column with polynomial fits. Band dispersion is given as τ, or the standard deviation of the band in seconds. □ represent τ for runs at 140 atm inlet pressure; △ at 175 atm; and ◇ at 250 atm.

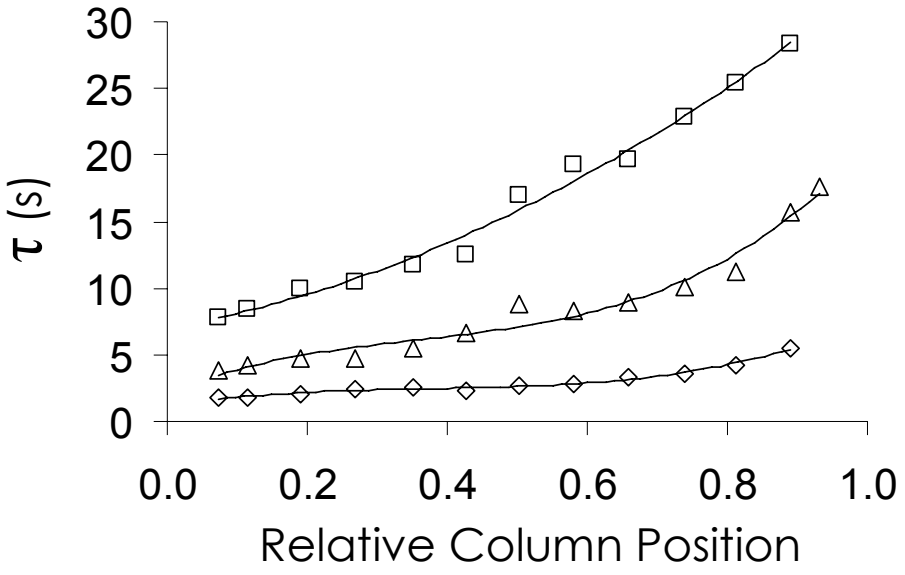

Figure 1B Temporal band dispersion profiles of phenanthrene in an SGC column with polynomial fits. Band dispersion is given as τ, or the standard deviation of the band in seconds. □ represent τ for runs at 140 atm inlet pressure; △ at 175 atm; and ◇ at 250 atm.

To predict theoretical values for local plate height, I employed the plate height equation for packed columns developed by Horvath and Lin [14]

$$H_i = \frac{A \cdot f_1(\rho)}{F_e} + \frac{B \cdot d_p}{1 + \frac{\omega}{d_p^{1/3} \cdot F_e^{1/3} \cdot f_2(\rho)}} + C \cdot d_p^2 \cdot F_e \cdot f_3(\rho) + D \cdot d_p^{5/3} \cdot F_e^{2/3} \cdot f_4(\rho) \quad (3)$$

where A, B, C, and D depend on constant column parameters, and $f_{1-4}(\rho)$ contain density dependent terms. F_e is the mass flow rate per unit area in the excluded or mobile zone and is given by

$$F_e = \frac{4m_f}{\pi \cdot d_c^2 \cdot \varepsilon_e} \quad (4)$$

where ε_e is the interparticle porosity. For columns randomly packed with spherical particles, ε_e is approximately 0.4 [14]. The value of ω is discussed shortly.

Expressions for A, B, C, and D are given below. A is defined as

$$A = 2\gamma \quad (5)$$

where γ is the obstructive factor of the column. For columns packed with solid spheres, γ is 0.65; however, for porous particles, γ may approach 1 [15]. I found that varying the value of γ between 0.65 and 1 had little effect on the theoretical efficiency; in the reported profiles, I assigned γ a value of 0.8.

The second constant term, B, is defined as

$$B = 2\lambda \quad (6)$$

where λ and ω are structural column parameters. For a reversed phase column packed with microparticles, Horvath and Lin [19] assigned λ and ω values of 2.5 and 2, respectively.

The third constant term, C, is defined as

$$C = \frac{\theta}{30\varphi \cdot (1+\varphi)^2} \tag{7}$$

where θ is the column tortuosity factor and φ is the ratio of the intraparticle volume accessible to the solute over the interstitial void volume. Horvath and Lin [14] suggest 2 as the value for θ. They also reported that for columns packed with porous microparticles, φ ranges between 0.5 and 1.0; however, they note that within this range the effect of φ on plate height is negligible. In my calculations I use 0.7 as the value for φ for both naphthalene and phenanthrene.

Finally, D is defined as

$$D = \frac{\kappa}{(1+\varphi)^2} \tag{8}$$

where κ is a structural parameter of the column. For columns with an interparticle porosity of 0.4, κ is approximately 1/15 [14].

Expressions for the density dependent terms, $f_{1-4}(\rho)$, in the Horvath-Lin equation are given as follows

$$f_1(\rho) = D_m \cdot \rho \tag{9}$$

where D_m is the diffusion coefficient of the analyte in the mobile phase. D_m can be calculated from the Wilke and Chang [16] equation which has previously been shown [12, 17] to be accurate for diffusion in supercritical CO_2

$$D_m = 7.4 \times 10^{-8} \cdot \frac{M_b^{1/2} \cdot T}{\eta \cdot V_a^{0.6}} \tag{10}$$

where M_b is the molecular mass of the mobile phase, T is the absolute temperature, η is the fluid viscosity, and V_a is the molar volume of the analyte at its boiling point.

Viscosity was determined using equation (2) from the previous chapter. Molar volumes for naphthalene and phenanthrene were taken from Le Bas [18].

The other density dependent terms are

$$f_2(\rho) = (D_m \cdot \rho)^{-1/3} \tag{11}$$

$$f_3(\rho) = \frac{(\varphi + k' + \varphi \cdot k')^2}{D_m \cdot \rho \cdot (1 + k')^2} \tag{12}$$

and

$$f_4(\rho) = \frac{(\varphi + k' + \varphi \cdot k')^2}{(D_m \cdot \rho)^{2/3} \cdot (1 + k')^2} \tag{13}$$

where k′ is the retention factor of the analyte and is strongly dependent on mobile phase density.

Combining knowledge of the mobile phase density gradient with the elution profiles of naphthalene and phenanthrene allowed me to calculate retention factors as a function of density. The local retention factor, k_i', of an analyte is defined as

$$k_i' = \frac{t_{R,i} - t_{m,i}}{t_{m,i}} \tag{14}$$

where $t_{R,i}$ and $t_{m,i}$ are the residence times in segment i of the analyte and an unretained component, respectively.

Values for $t_{m,i}$ can be obtained from the column density profile

$$t_{m.i} = \frac{dL}{u_{m,i}} \tag{15}$$

where $u_{m,i}$ is the velocity of the unretained component in the i^{th} segment and dL is the length of the segment. Assuming that the unretained component is fully penetrating, its velocity is given by

$$u_{m,i} = \frac{4m_f}{\pi \cdot d_c^2 \cdot \rho_i \cdot \varepsilon_t} \quad (16)$$

where ρ_i is the mobile phase density in the i^{th} segment and ε_t is the total column porosity. As noted in paper one, the total column porosity was 0.7 as determined by the gravimetric method [19].

Using equations (15) and (16), I calculated $t_{m,i}$ as a function of column position. Combining these values with the elution profiles of naphthalene and phenanthrene reported previously, I calculated retention factors as a function of mobile phase density. For isothermal separations the dependence of retention factor on mobile phase density is given by

$$\ln(k') = a + b \cdot \rho + c \cdot \rho^2 \quad (17)$$

where a, b, and c are empirical coefficients [20, 21]. These coefficients for naphthalene and phenanthrene at 130 °C are given in Table I.

Table I

Coefficients relating retention factor, k′, of naphthalene and phenanthrene to mobile phase density based on the relation: $\ln(k') = a + b \cdot \rho + c \cdot \rho^2$

	a	**b**	**c**
Naphthalene	4.934	−13.105	9.989
Phenanthrene	8.173	−18.443	8.173

Knowing the mobile phase density and the analyte retention factors as a function of column position, I used equation (3) to predict the local efficiencies of naphthalene and phenanthrene with respect to position in an SGC column operating at 140, 175, and 250 atm inlet pressures. A comparison of the experimental and theoretical column efficiency profiles for naphthalene and phenanthrene are shown in Figure 2.

The theoretical density profiles predict that efficiency decreases only gradually along the column, until just prior to the column outlet, where significant band broadening is expected. Figure 3 shows the velocity profile of the mobile zone for an inlet pressure of 250 atm. The mobile zone velocity is calculated using equation (16), except that the total column porosity, ε_t, is replaced with the porosity of the excluded region, ε_e. It can be seen that the theoretical plate height profiles closely parallel the linear velocity of the mobile zone. This suggests that column pressure drop is not directly responsible for efficiency loss, but rather high mobile phase flow rates near the column outlet can cause band broadening if the absolute density is allowed to drop too low.

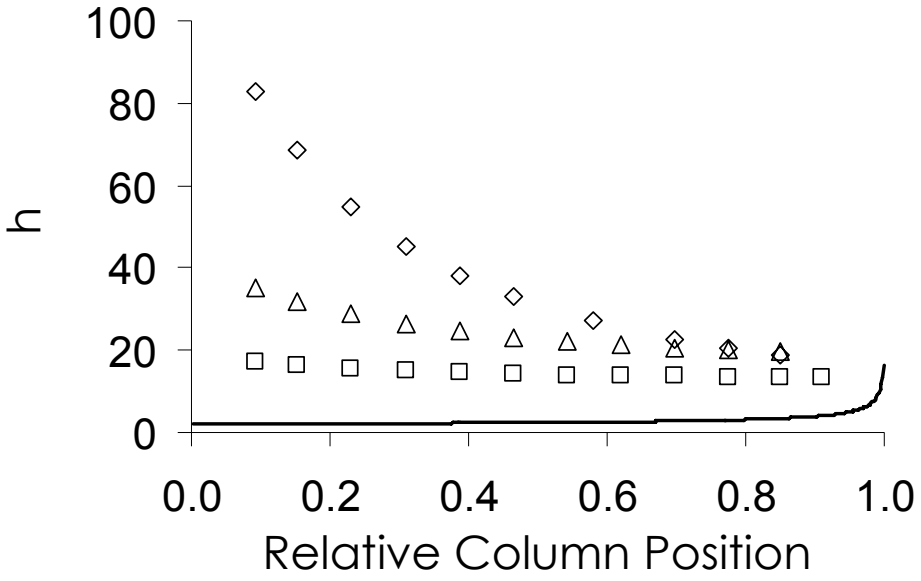

Figure 2A Column efficiency profiles for naphthalene given as the local reduced plate height, h, with respect to column position. □ represent h for runs at 140 atm inlet pressure; △ at 175 atm; and ◇ at 250 atm. The solid line represents the theoretical efficiency profile calculated for an inlet pressure of 250 atm.

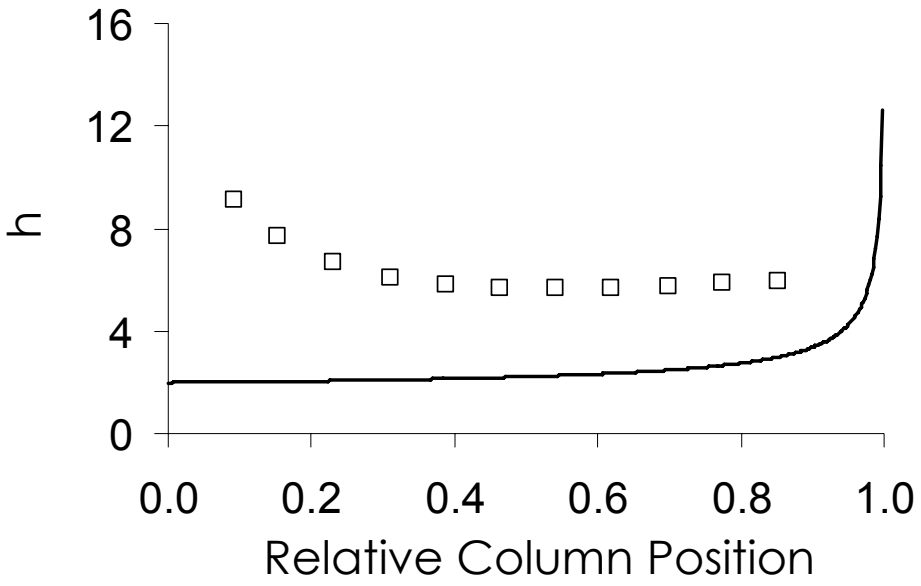

Figure 2B Column efficiency profiles for phenanthrene at 140 atm inlet pressure given as the local reduced plate height, h, with respect to column position. The solid line represents the theoretical efficiency profile.

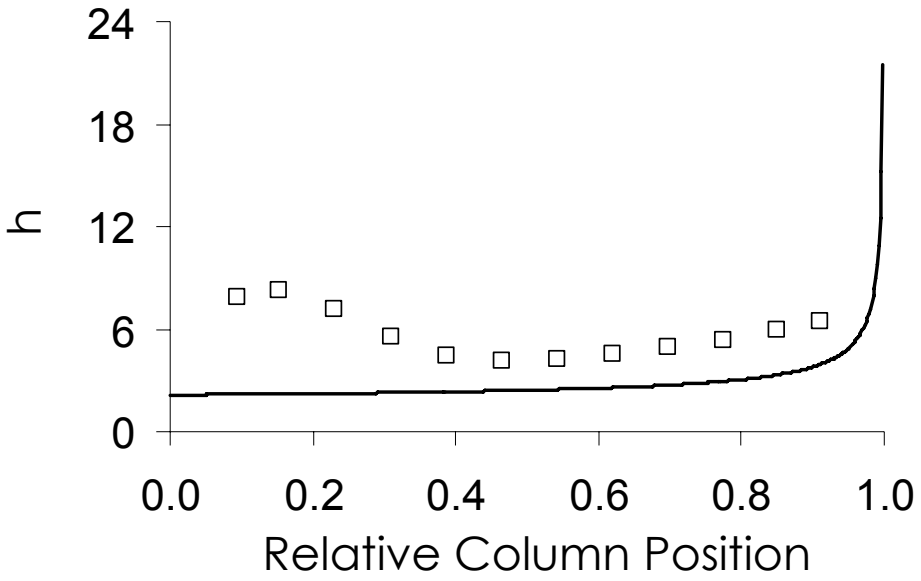

Figure 2C Column efficiency profiles for phenanthrene at 175 atm inlet pressure given as the local reduced plate height, h, with respect to column position. The solid line represents the theoretical efficiency profile.

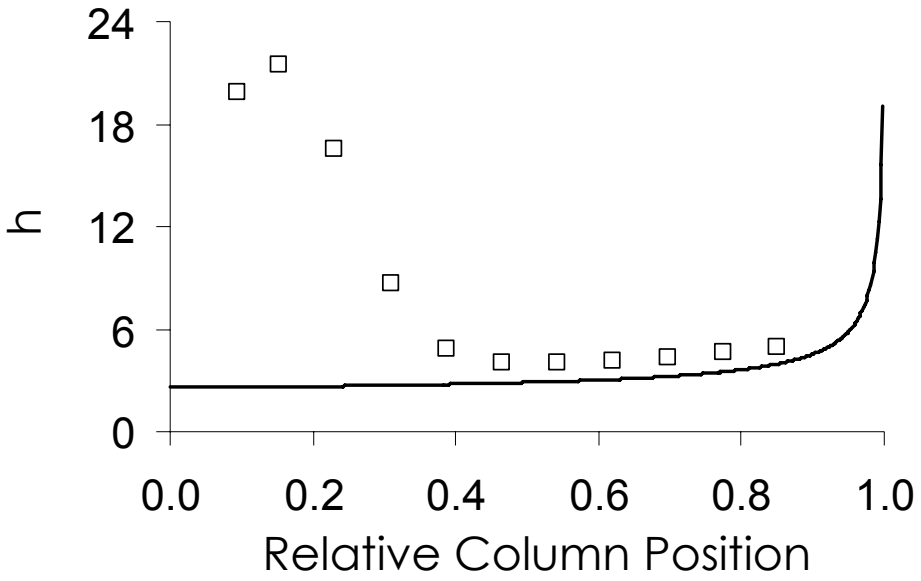

Figure 2D Column efficiency profiles for phenanthrene at 250 atm inlet pressure given as the local reduced plate height, h, with respect to column position. The solid line represents the theoretical efficiency profile.

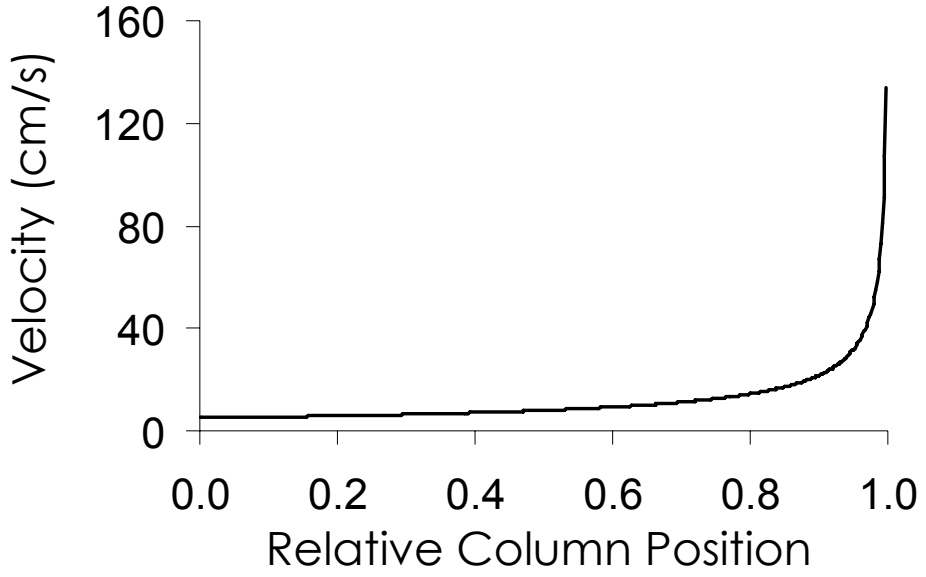

Figure 3 Mobile zone velocity, u_e, as a function of column position, calculated from the mobile phase density profile for an SGC column operating at 250 atm inlet pressure. It is seen that the theoretical efficiency profiles shown in Figure 2 closely follow the mobile phase velocity, indicating that high linear velocities are responsible for band broadening near the column outlet.

The experimental efficiency for naphthalene is much worse than the model predicts. The efficiency is poorest at the column inlet, but gradually improves over the length of the column. Additionally, the deviation from theoretical plate height for naphthalene increases with increasing column inlet pressure. In the case of phenanthrene, the experimental efficiency appears to correlate well with the model. Exceptions are observed at the column inlet of the 175 and 250 atm runs, where efficiency is poor over the first 10 cm of the column, but quickly recovers. As seen with naphthalene, this additional band broadening is worse at the higher inlet pressure. Figure 4 shows the elution for naphthalene and phenanthrene with respect to column position. It can be seen that the additional band broadening closely correlates with high analyte elution rates and appears to only occur when the analyte is migrating faster than approximately 0.15 cm/s.

It is likely that radial temperature gradients contributed to band broadening in these experiments. A series of studies by Poe and coworkers [24, 25] gave evidence for the formation of radial temperature gradients in packed capillaries due to Joule-Thomson cooling of the mobile phase. Because the columns are externally heated, the perimeter remains warm while the interior cools due mobile phase expansion. Poe and coworkers [24, 25] showed that these radial temperature gradients can result in a loss of efficiency for columns operating across a large density gradient. However, this broadening mechanism predicts the poorest efficiency to occur near the column outlet where the mobile phase expansion is greatest. This does not fit with my results which show the greatest band broadening near the column inlet, indicating that another mechanism must be responsible for the observed loss in efficiency.

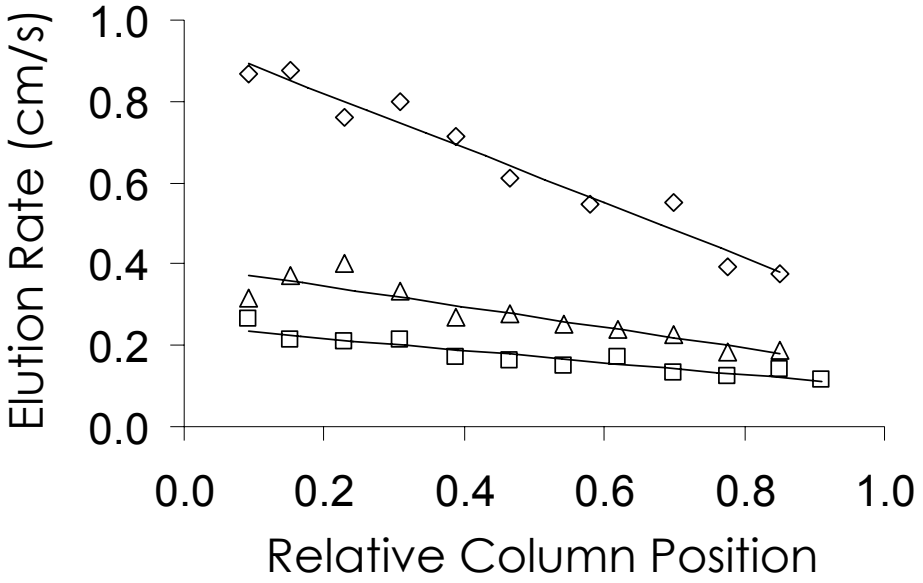

Figure 4A Elution rate profiles of naphthalene in an SGC column operating at inlet pressures of 140 (□), 175 (△), and 250 (◇) atm.

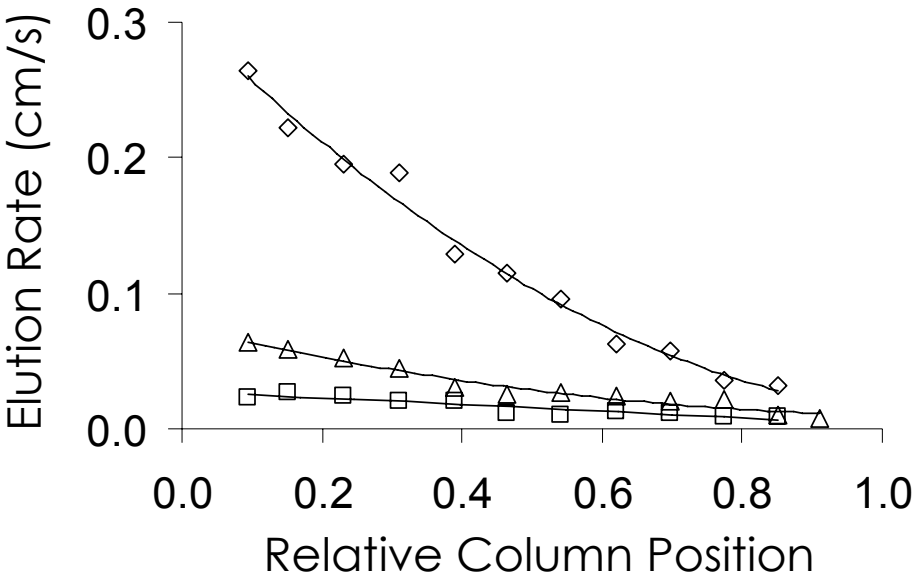

Figure 4B Elution rate profiles of phenanthrene in an SGC column operating at inlet pressures of 140 (□), 175 (△), and 250 (◇) atm. A strong correlation is visible between high analyte velocities (>0.15 cm/s) and poor observed efficiency shown in Figure 2.

I offer the following as a possible explanation for the observed band broadening. Strubinger and Parcher [22] have shown that under certain conditions, CO_2 can form a thick film inside the stationary phase on the silica support. Berger [23] hypothesized that one reason for band broadening in supercritical fluid separations could be the shearing of this film at high flow rate. This hypothesis fits well with my observations which showed increased band broadening with higher inlet pressures. In the case of strong interactions between the analyte and the stationary phase, shearing of the CO_2 film would be less likely to cause band broadening, because strong interactions would ensure that the analyte remains adsorbed to the stationary phase rather than shear with the film. This could explain why the observed band broadening was worse for naphthalene than phenanthrene and improved as column density dropped and retention increased.

Band Focusing

An additional effect of the column density gradient in SGC is band focusing. When a band velocity gradient exists, the front of the band moves either more slowly or more quickly than the back of the band, resulting in band compression or band expansion. The relationship between the temporal and the spatial dispersion is given by

$$\tau_i = \sigma_i \cdot \left\langle \frac{1}{u_R} \right\rangle_z \tag{18}$$

where τ_i is the observed temporal dispersion in segment i, σ_i is the corresponding spatial dispersion, u_R is the band velocity, and $< >_z$ represents a spatial average over the length σ_i. If I assume that the band velocity is nearly constant over the length σ_i, then I can approximate the spatial dispersion as

$$\sigma_i \approx \tau_i \cdot u_{R,i} \tag{19}$$

Using equation (19), I calculated the spatial dispersion of the band as a function of column position using the polynomial fits to the temporal dispersion and the analyte velocity profiles shown above. These spatial dispersion profiles are shown in Figure 5. As expected, the band focusing is greater for phenanthrene than naphthalene. Additionally, it can be seen that the band compression becomes more pronounced at higher inlet pressures where the density gradient is steeper.

The effects of band focusing on separation performance have been discussed in depth by Blumberg and others [26–32]. In the case of SFC or SGC, the density gradient forms what has been termed a nonuniform, time-invariant separation [26]. Nonuniform refers to the spatial gradient, indicating that column parameters vary with respect to column position. Time-invariant indicates that the column parameters are not changing with respect to time. This type of separation can produce focusing of the band spatially. Assuming no column contribution to band broadening, this spatial focusing is described by

$$\sigma_f = \left(\frac{u_{R,f}}{u_{R,o}} \right) \cdot \sigma_o \tag{20}$$

where σ_f is the final spatial dispersion of the band, σ_o is the spatial band dispersion at the time of injection, and $u_{R,f}$ and $u_{R,o}$ are the final and initial band velocities, respectively.

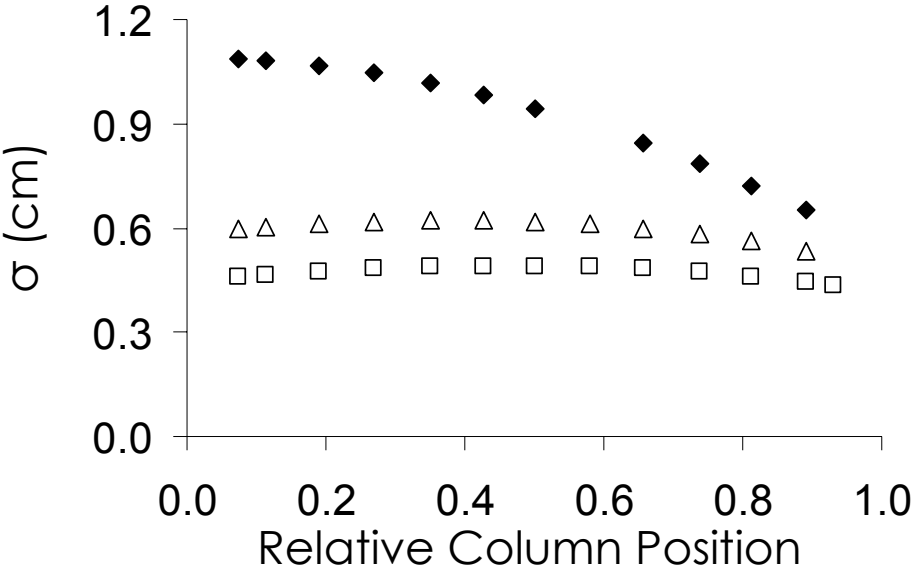

Figure 5A Naphthalene spatial dispersion profiles in an SGC column. Band dispersion is given as σ, or the standard deviation of the band in cm. □ represent σ for runs at 140 atm inlet pressure; △ at 175 atm; and ◇ at 250 atm. Band focusing is observed at 250 atm inlet pressure where the density gradient is steepest.

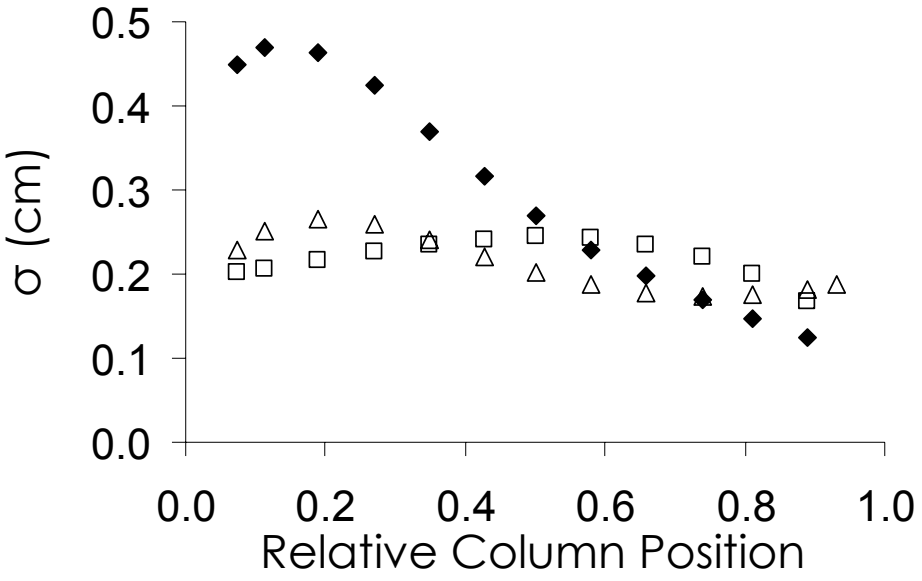

Figure 5B Phenanthrene spatial dispersion profiles in an SGC column. Band dispersion is given as σ, or the standard deviation of the band in cm. □ represent σ for runs at 140 atm inlet pressure; △ at 175 atm; and ◇ at 250 atm. As with naphthalene, band focusing is observed at 250 atm inlet pressure where the density gradient is steepest.

However, band width is observed as the time required for the analyte to pass the detector, and the slower the band moves through the detector, the wider it will appear. If I assume that the entire length of the band is moving with a uniform velocity at the time it is injected and at the time it is detected, I can show that

$$\tau_f = \frac{\sigma_f}{u_{R,f}} \tag{21}$$

where τ_f is the final temporal dispersion of the band. Substituting equation (30) into this expression yields

$$\tau_f = \frac{\sigma_o}{u_{R,o}} = \tau_o \tag{22}$$

Here it can be seen that the band dispersion remains unchanged in time despite spatial focusing. This means that although the band focuses spatially, this focusing cannot be observed when detecting in time because spatial focusing is offset by the decrease in band velocity.

Although spatial band focusing in a nonuniform, time-invariant separation does not lead to an improvement in observed efficiency, it can still be advantageous for several reasons. First, band compression results in increased analyte concentration that can lead to improved signal-to-noise for concentration sensitive detectors. Here I define a concentration sensitive detector as a detector in which the response is proportional to the concentration of analyte inside a detector cell as opposed to the mass flow rate of analyte through the detector cell [33]. Any type of optical detector, such as the fluorescence detector employed in this study, can be classified as a concentration sensitive detector. Second, Blumberg demonstrated that a negative band velocity gradient can help a separation recover from the effects of poor sample introduction [28, 29].

Finally, if the spatial gradient is combined with a temporal gradient, then increased separation efficiency can be observed. The question of whether this improvement in efficiency can result in increased resolution or peak capacity has been the subject of controversy [26–32]. Recent results by Contreras et al. [32] suggest that a moving thermal gradient can increase the peak capacity of GC relative to traditional time-based temperature programming. It is possible to develop analogs to a moving thermal gradient in GC for supercritical fluid separations. Such analogs could be achieved by combining the mobile phase density gradient with a time-based temperature program or by using a back-pressure regulated flow restrictor for density gradient programming.

Conclusions

Modeling plate height with respect to column position in an SGC column shows no significant loss of efficiency with pressure drop. Rather, theoretical band broadening can be correlated to the high flow rates that occur near the column outlet. In theory, fast, high efficiency separations are achievable when operating across a large pressure drop, as long as the column outlet pressure is not allowed to drop too low. Operating the column at higher inlet pressures in combination with a moderate flow restrictor should allow for equally high mass flow rates, with a greatly reduced linear velocity near the column outlet. Such a separation would be expected to be faster and more efficient than typical SGC, especially for low-volatility compounds.

In addition to theoretical modeling, on-column monitoring of band dispersion provided a direct measure of local column efficiency. These measurements showed substantial band broadening not predicted by theory, and this effect was correlated to regions of high analyte velocity (>0.15 cm/s). I hypothesize that these observations

support an earlier hypothesis by Berger [23] that shearing of a film of CO_2 that forms around the silica base of the stationary phase contributes to band broadening. Future work is necessary to test this hypothesis.

I also observed spatial band focusing resulting from the band velocity gradient. I believe that this focusing effect could be utilized to improve the peak capacity of supercritical fluid separations. By combining the column density gradient with a time-based program, the bands could focus spatially as they move down the density gradient and then be swept quickly to the detector in time. This type of technique would also be useful for analysis of targeted compounds. Peak sweeping could be accomplished using a temperature program or a back-pressure regulated, variable flow restrictor for density gradient programming.

Finally, on-column analysis has been shown to be a useful tool for studying gradient separations. In this study, on-column detection provided a direct measurement of mobile phase density, analyte retention, and separation efficiency as a function of column position. This allowed for changes in separation speed and efficiency to be correlated more accurately with local column conditions.

References

[1] J.C. Giddings, Anal. Chem. 36 (1964) 741.

[2] M.N. Meyers, J.C. Giddings, Anal. Chem. 37 (1965) 1453.

[3] S.M. Fields, M.L. Lee, J. Chromatogr. 349 (1885) 305.

[4] P.J. Schoenmakers, F.C.J.G. Verhoeven, J. Chromatogr. 352 (1986) 315.

[5] K.D. Bartle, T. Boddington, A.A. Clifford, G.F. Shilstone, J. Chromatogr. 471 (1989) 347.

[6] P.J. Shoenmakers, L.G.M. Uunk, Chromatographia, 24 (1987) 51.

[7] P.A. Mourier, M.H. Caude, R.H. Rosset, Chromatographia, 23 (1987) 21.

[8] D.R. Gere, R. Board, D. McManigill, Anal. Chem. 54 (1982) 736.

[9] T.A. Berger, J.F. Deye, Chromatographia, 30 (1990) 57.

[10] C.A. Cramers, P.A. Leclercq, J. Chromatogr. A. 842 (1999) 3.

[11] D.P. Poe, D.E. Martire, J. Chromatogr. 517 (1990) 3.

[12] H.G. Janssen, H.M.J. Snijders, J.A. Rijks, C.A. Cramers, P.J. Schoenmakers, J. High Resolut. Chromatogr. 14 (1991) 438.

[13] J.C. Giddings, Unified Separation Science. John Wiley and Sons, Inc., New York, 1991.

[14] Cs. Horvath, H.-J. Lin, J. Chromatogr. 149 (1978) 43.

[15] J.H. Knox, H.P. Scott, J. Chromatogr. 282 (1983) 297.

[16] R.C. Reid, J.M. Prausnitz, T.K. Sherwood, The properties of Gases and Liquids, 3rd Ed. McGraw Hill, New York, 1977.

[17] H.G. Janssen, J.A. Rijks, C.A. Cramers, J. Microcolumn Separations 2 (1990) 26.

[18] G. Le Bas, The Molecular Volumes of Liquid and Chemical Compounds. Longmans, Green and Co., London, 1915.

[19] G.E. Berendsen, P.J. Schoenmakers, L. De Galan, G. Vigh, Z. Varga-Puchony, J. Inczedy, J. Liq. Chromatogr. 3 (1981) 13.

[20] D.E. Martire, J. Chromatogr. 461 (1989) 165.

[21] R.L. Riester, T.J. Bruno, A. Hussam, D.P. Poe, D.E. Martire, J. Chromatogr. 545 (1991) 135.

[22] J.R. Strubinger, H. Song, J.F. Parcher, Anal. Chem. 63 (1991) 98.

[23] T.A. Berger, J.F. Deye, Chromatographia 37 (1993) 645.

[24] D.P. Poe, J. Chromatogr. A. 785 (1997) 129.

[25] X. Wensheng, D.L. Peterson, J.J. Shroden, D.P. Poe, J. Chromatogr. A. 1078 (2005) 162.

[26] L.M. Blumberg, Anal. Chem. 64 (1992) 2459.

[27] L.M. Blumberg, Chromatographia 39 (1994) 719.

[28] L.M. Blumberg, J. Chromatogr. Sci. 35 (1997) 451.

[29] L.M. Blumberg, T.A. Berger, J. Chromatogr. 596 (1992) 1.

[30] J.B. Phillips, V. Jain, J. Chromatogr. Sci. 33 (1995) 541.

[31] V. Jain, J.B. Phillips, J. Chromatogr. Sci. 33 (1995) 601.

[32] J.A. Contreras, H.D. Tolley, M.L. Lee, Use of Axial Temperature Gradients in Gas Chromatography. Presented at Pittsburgh Conference on Analytical Chemistry and Applied Spectroscopy, New Orleans, LA, 2008. Paper 170-7.

[33] M.L. Lee, Fundamentals of Analytical Separations. BYU Academic Publishers, 2008.

Chapter 4: Effects of Solvent Pressure on the Structure of Model C18 Stationary Phases Studied by Sum-Frequency Generation Spectroscopy

Abstract

The shape selectivity of stationary phases is known to be closely linked to structure. Although liquid chromatography (LC) and supercritical fluid chromatography (SFC) are performed at high pressures, little work has been done to characterize the effects of pressure on stationary phase structure, even though the literature reports several examples of pressure-induced changes in stationary phase selectivity. In this work, I report direct observations of C18 monomeric and polymeric stationary phase model systems in water at pressures up to 60 atm using sum-frequency generation spectroscopy. Spectral changes are correlated with pressure-induced structural changes in the C18 phases. These observations provide a basis for correlating column pressure with selectivity in LC and SFC separations.

Introduction

Retention in chromatography is an active process, described by solvent-solvent interactions, solvent-analyte interactions, and analyte-stationary phase interactions. Originally, it was supposed that the stationary phase played a passive role, only providing adsorption sites for analyte molecules; this is known as the solvophobic theory of retention [1]. According to the solvophobic theory, retention can be given in terms of the free energy barrier to formation of a solute-sized hole in the mobile phase. Although this theory is useful for considering the contribution of adsorption to analyte retention, this picture of chromatography is incomplete and fails to predict shape selectivity.

Observations of shape selectivity of polycyclic aromatic hydrocarbons (PAH) gave rise to partition theories in chromatography where the stationary phase plays an active role in retention [2]. It has been shown theoretically that entropic forces in the stationary phase can control incorporation and expulsion of analyte from the film [3], and it is widely accepted that solute partitioning is the dominate retention mechanism for small, non-polar molecules in reversed phase separations [4].

According to the partition theory of retention, structure of the stationary phase is closely linked to selectivity. Martire and coworkers [5] showed theoretically that enhanced shape selectivity is expected when an isotropic, or randomly ordered, stationary phase is replaced by an anisotropic, or orientationally ordered, stationary phase, and numerous experiments have verified this model [6–8]. Liquid crystalline stationary phases are often used for separating isomers because their highly ordered structures allow for shape selective partitioning of isomers [5]. Williams et al. [9] studied the shape selectivity of monomeric and polymeric C18 phases for the separation of PAH isomers, and showed that shape selectivity increases with conformational ordering.

Solvent environment, coverage density, and chain length of the stationary phase have been observed to affect the selectivity [10–17], and a number of studies have been performed to link these column parameters to changes in conformational ordering of the stationary phase. Lu and Rutan [11] characterized the structure of a derivatized C18 stationary phase with changing solvent environment. They found that the structure strongly depends on solvent composition, and characterized three distinct stationary phase conformations. Martire and Boehm [10] observed that the selectivity of alkylsilane stationary phases increased with increasing chain length and attributed this effect to

increased conformational ordering of the longer chains due to steric effects. Messmer and coworkers [12–16] studied the conformation of monomeric and polymeric C18 models using sum-frequency generation (SFG) spectroscopy. They concluded that in addition to solvent composition, the structure of the stationary phase also depends strongly on the coverage density of the stationary phase and on the degree of cross-linking between alkyl chains.

A number of studies have also linked pressure to changes in selectivity [18–20]. Gritti et al. [19] studied the effect of temperature and pressure on the selectivity of liquid crystals in SFC. They found that the selectivity dependence on temperature was opposite, depending on if the column was at low or high pressure. They also observed greater selectivity at low pressure than at high pressure. In this work, they explained these observations in terms of retention shifts resulting from changing fluid density. Ponton et al. [18] investigated the effect of average column pressure on chiral selectivity in LC using a C18 stationary phase and a cyclodextrin additive. They found that in certain instances the order of elution could be reversed by changing the average column pressure. They attributed this effect to a shift in binding equilibrium of the analyte with the additive due to pressured-induced changes in partial molar volumes.

Little work has been done to link the effects of pressure on stationary phase performance with pressure-induced structural changes in the stationary phase. Liao et al. [21] used Raman spectroscopy to observe the effect of pressure on the relative order of monomeric and polymeric C18 stationary phases. In their experiments, they exposed a column to pressure under a variety of solvent compositions for an extended period of time. They also used control columns in which the solvent environment was kept the

same, but no pressure was applied. After depressurizing the column, they made measurements of relative order of the alkyl chains using Raman spectroscopy. They found that the pressurized stationary phases showed slightly greater disorder than the control phases following pressure treatment and that the pressure induced changes were more pronounced for polymeric phases. However, because no measurements were made while the stationary phase was still under pressure, the real-time effects of pressure could not be observed. Consequently, these results are limited to characterizing the irreversible effects of the pressure treatment.

In this study I employ SFG spectroscopy to actively probe the structure of monomeric and polymeric C18 models in aqueous environment at pressures up to 60 atm. These spectra represent the first direct observations of alkylsilanes while under pressure and provide a more accurate understanding of the effect of column parameters on the structure and performance of stationary phase materials.

Experimental

SFG Experiments

To obtain SFG spectra of alkylsilanes under pressure, I first prepared model stationary phases on fused silica windows as described below. These windows were then placed in a cell that allowed for control of solvent and pressure. SFG spectra were collected by probing through the window; this allowed me to obtain spectra of the C18 model on the inner surface of the substrate. A diagram of the pressure cell is shown in Figure 1.

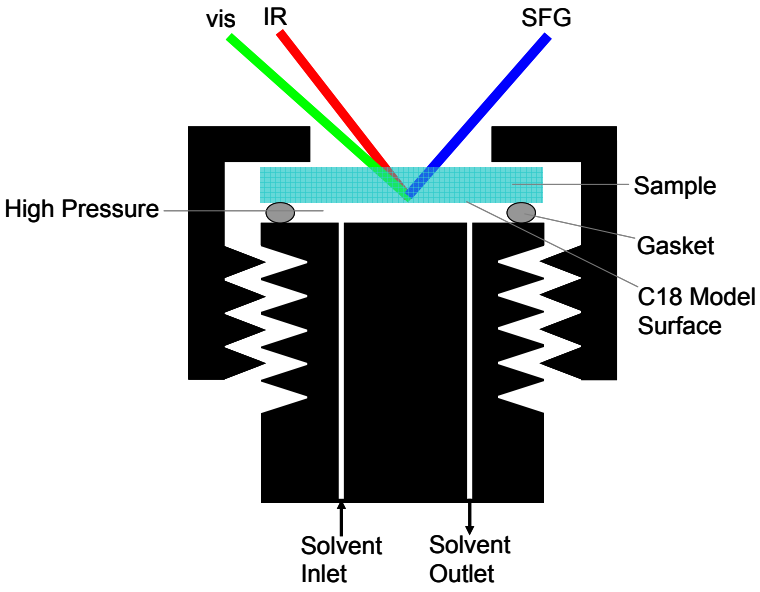

Figure 1 Diagram of the cell that allowed the solvent and pressure environment of the sample to be controlled while probing the C18 model surface using SFG. The solvent inlet was connected to an SFC pump to generate high pressures. The model phase was probed through the back surface of the sample window. A needle valve was connected to the solvent outlet that could be opened to flush the cell or closed to pressurize the cell.

Pressure behind the sample window was controlled using an SFC pump (Lee Scientific). The pump was equipped with a digital pressure transducer and feedback mechanism that enabled the pump to maintain a constant pressure. Connections to the inlet and outlet of the cell were made using NPT-to-Swage adapters. The pump was connected to the solvent inlet of the cell, and a needle valve (HIP) was placed at the solvent outlet.

Figure 2 shows a diagram of the laser system and spectrometer used to collect SFG spectra. A portion of the 800 nm beam from an ultrafast laser (Integra-C, Quantronix) was used to pump an OPA (Topas, Quantronix) to produce a broadband IR beam. The remaining 800 nm light was used as the visible beam for SFG. This beam was spectrally narrowed using a Fabry-Perot etalon. A delay path allowed for the visible beam to be overlapped in time with the IR beam. Two periscopes acted as polarization selectors for the visible and IR light. The beams were focused by two separate lenses and combined at the sample in a nearly collinear geometry. The beams were incident on the sample at 60° relative to the sample normal.

The SFG signal was collected with a collimating lens and passed through a short-pass filter to remove the 800 nm beam, which was nearly collinear with the sum-frequency beam. A half-wave plate allowed the signal to be rotated to match the polarization preference of the spectrometer. An f-matching lens focused the signal into the spectrometer (Shamrock sr-303i, Andor). The width of the entrance slit was set between 175 and 200 μm. Spectra were collected in ssp polarization where this notation specifies the polarization states of the sum-frequency, visible, and IR beams,

respectively. Integration times ranged from five to seven minutes. Curve fitting for spectral analysis was done using Grams/32 (Galactic Industries Co.) software.

Sample Preparation

Model monomeric and polymeric C18 stationary phases were synthesized on fused silica windows (ChemGlass). Prior to the synthesis, the windows were cleaned for 1 h in piranha solution (1:1 mixture of 30% H_2O_2 and concentrated H_2SO_4), rinsed with water, activated in a vacuum oven at 80 °C and 5 in. Hg for 12 h, and allowed to cool in a vacuum desicator. Care must be taken in cleaning the slides because piranha solution is highly corrosive.

Syntheses of the monomeric and polymeric C18 phases were performed under N_2 atmosphere. For the monomeric synthesis, 30 mL of anhydrous toluene were transferred to a 500 mL round bottom flask, and the window was immersed in the toluene. Between 0.25 and 0.30 g of chlorodimethyloctadecylsilane (Aldrich) and 250 μL of ethylenediamine (Aldrich) were transferred to the flask. The flask was then topped with a glass stopper and shaken at 100 rpm for 72 h.

For the polymeric phase synthesis, 20 mL of HPLC grade methylene chloride were added to the 500 mL round bottom flask. The window was then immersed in the solvent and 200 μL of trichlorooctadecylsilane (Aldrich) were added. The flask was stopped with a glass stopper and shaken at 100 rpm for 12 h.

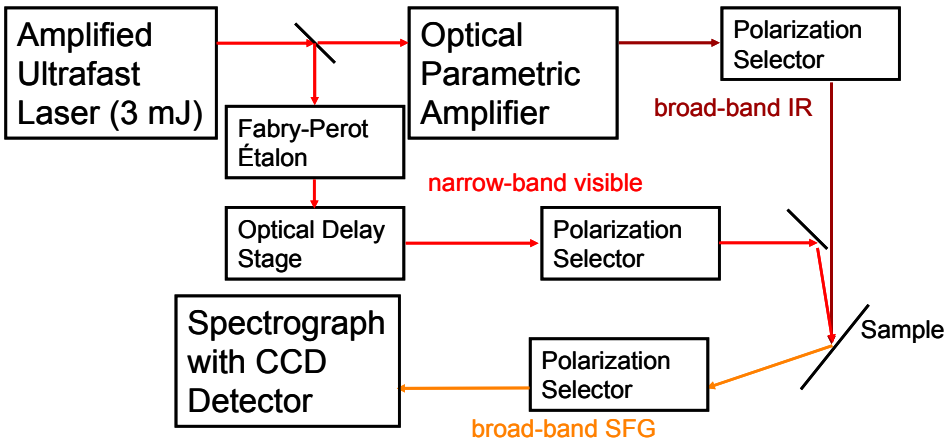

Figure 2 Beam schematic for generating and detecting sum-frequency signal. The OPA generated a broadband IR pulse. The Fabry-Perot etalon spectrally narrowed the visible beam. Periscopes acted as polarization selectors for the IR and visible beams, and a quarter-wave plate and spectrometer acted as the polarization selector for the SFG signal.

Following synthesis, the window was rinsed twice with reagent grade hexanes, once with HPLC grade methanol, once with distilled water, and then again with methanol. The window was then dried under a gentle stream of N_2 and analyzed by contact angle measurements. The standing contact angle of water was measured at 5 places on each slide using a contact angle goniometer (Ramè-Hart, Inc.). For the monomeric samples, the contact angle was 105 ±5°, and for the polymeric samples, the contact angle was 135 ±15°. The samples were stored in HPLC grade methanol until use.

The synthesis produced a C18 phase on both sides of the window. To prevent absorption of the IR beam by the alkyl chains on the back surface of the window during SFG experiments, the C18 phase on this side was removed by rubbing it with a cotton swab dipped in 2 M NaOH. Contact angle measurements of the back side following this treatment showed that water easily wet the surface, indicating that the NaOH had hydrolyzed the alkysilanes. Contact angle measurements of the front side of the window following this treatment showed that the contact angle was unchanged, verifying that the treatment had not damaged the C18 phase on the front surface.

When ready for use, the window was removed from the methanol and placed in the pressure cell. A spectrum of the sample was obtained in air, prior to introducing water into the pressure cell. About 3 mL of water (18 MΩ) were then flushed from the pump through the cell. The needle valve at the solvent outlet was then closed, and spectra were taken of the sample at 10 atm increments from ambient pressure to 60 atm. I was unable to observe spectra above 60 atm because higher pressures caused the windows to break.

Spectral Analysis

The following peak assignments were used in this work as given in reference [12]: the band centered at 2850 cm^{-1} is the symmetric methylene stretch; the band centered at 2910 cm^{-1} is the symmetric methyl stretch; and the band centered at 2950 cm^{-1} is the asymmetric methylene stretch. For a qualitative structural analysis, I consider the relative intensities of these bands. The intensity of the symmetric methyl stretch provides a measure of the tilt of the terminal methyl groups on the C18 chains. In the ssp polarization, increased intensity of this stretch indicates that the C_{3v} axis of the methyl group is oriented normal to the sample surface, and decreased intensity indicates that the methyl C_{3v} axis is lying down parallel to the surface. The asymmetric methylene provides a measure of the relative orientation of the methylene groups in the C18, or the chain body. If the chains are standing upright, parallel to the surface normal, then the dipole moment of this vibration is oriented perpendicular to the p-polarized IR beam, and this stretch, to a first approximation, is not observed. The intensity of the stretch increases as the chain bodies lie down on the surface.

A measure of the degree of order in the alkyl chains can be given by the relative intensities of the symmetric methylene and the symmetric methyl stretches. As the chains order, the local environment of the methylene groups becomes centrosymmetric, so the intensity of the symmetric methylene stretch decreases. However, as the number of gauche conformations increase in the chains, the intensity of the symmetric methylene stretch increases relative to the symmetric methyl stretch. Accordingly, a disorder ratio, D, can be defined as

$$D = \frac{I_{CH_2sym}}{I_{CH_3sym}} \qquad (1)$$

where I_{CH_2sym} and I_{CH_3sym} are the intensities of the symmetric methylene and methyl stretches, respectively. I did not normalize these spectra based on the intensity profile of the IR envelope, so this analysis is limited to qualitative observations based on changes between spectra.

To calculate uncertainty in the disorder ratio, I relied on the standard error of the curve fits. The standard error is defined as the standard deviation of the residuals, and is calculated for each band. I approximate the degrees of freedom for the fit as

$$\mathrm{dof} = \frac{n - p}{b} \tag{2}$$

where dof is the degrees of freedom, n is the number of data points in the curve fit, p is the number of fitting parameters used, and b is the number of bands fit. Using this estimate for the degrees of freedom and the standard error, I calculated uncertainty at the 95% confidence level.

The spectra were collected in non-deuterated water. This was possible for two reasons. First, I was not probing through the solvent but rather through the back surface of the window. Second, the vibrational resonance of water does not overlap with the C-H stretch region which I observed in my experiments. A qualitative comparison of the data with previously obtained SFG spectra [12, 15, 17] indicate that IR absorption by the water does not affect the spectra.

Results and Discussion

Initially, I obtained spectra of model monomeric and polymeric phases in air at ambient pressure. These spectra are shown in Figure 3, and are qualitatively similar to spectra obtained by Horn [17] and by Messmer and coworkers [12, 15] for similar samples at the silica-air interface.

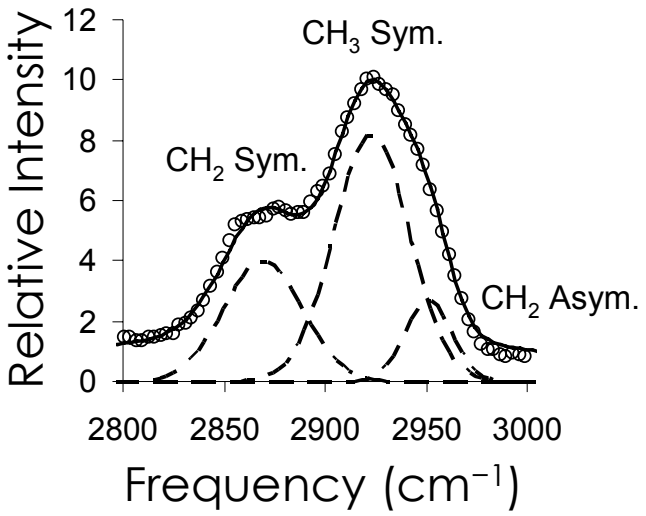

Figure 3A SFG spectrum of a monomeric sample in air at ambient pressure. The band to the left, centered at 2850 cm^{-1}, is the symmetric methylene stretch; the middle band, centered at 2910 cm^{-1}, is the symmetric methyl stretch; and the band to the right, centered at 2950 cm^{-1}, is the asymmetric methylene stretch.

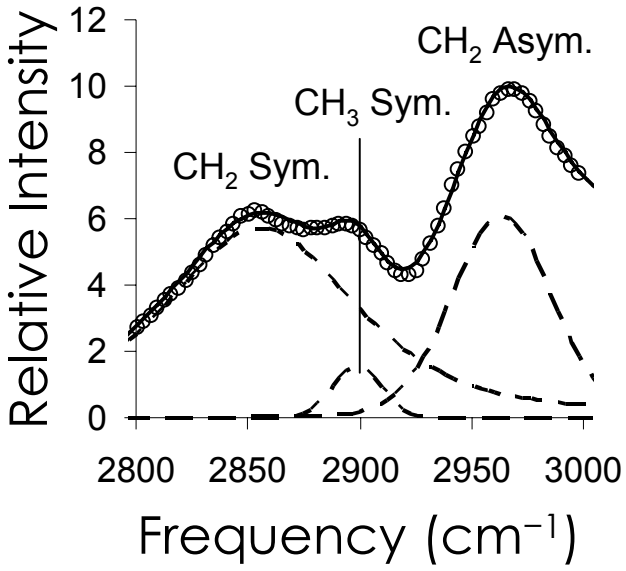

Figure 3B SFG spectrum of a polymeric sample in air at ambient pressure. The band to the left, centered at 2850 cm^{-1}, is the symmetric methylene stretch; the middle band, centered at 2910 cm^{-1}, is the symmetric methyl stretch; and the band to the right, centered at 2950 cm^{-1}, is the asymmetric methylene stretch.

Figure 4 shows spectra of the monomeric phase under water at various pressures ranging from ambient to 60 atm. The spectrum obtained at ambient pressure is qualitatively similar to spectra previously reported for the monomeric phase at the silica-water interface [12, 15]. The intensity of the asymmetric methylene stretch decreases as the sample goes from air to water and is not observed in any of the spectra taken at the silca-water interface. This indicates that the alkyl chains are tilting at some angle toward the surface when in air, but stand nearly straight up parallel to the surface normal when placed in water.

Figure 5 shows the disorder ratio of a monomeric sample for the spectrum obtained in air and for the spectra taken at the water interface as a function of pressure. The disorder ratio appears to fluctuate randomly around 0.6, indicating that pressure has a minimal effect on conformational order of the alkyl chains.

Figure 6 shows spectra of the polymeric phase under water at various pressures ranging from ambient to 60 atm. Again, the spectrum obtained at ambient pressure is similar to previously reported spectra for C18 polymeric phases at the silica-water interface [12, 17]. Comparison of Figure 3B with Figure 6A shows that the intensity of the symmetric methyl stretch increases significantly going from air to water. This indicates that the terminal methyl groups point upward along the surface normal when placed under water. This is similar to the behavior observed for the monomeric samples in which the alkyl chains stand upright when placed in water. These observations can be attributed to entropic forces in the water that cause the non-polar C18 phase to stand up and adopt a structure of minimum surface area when exposed to the polar solvent.

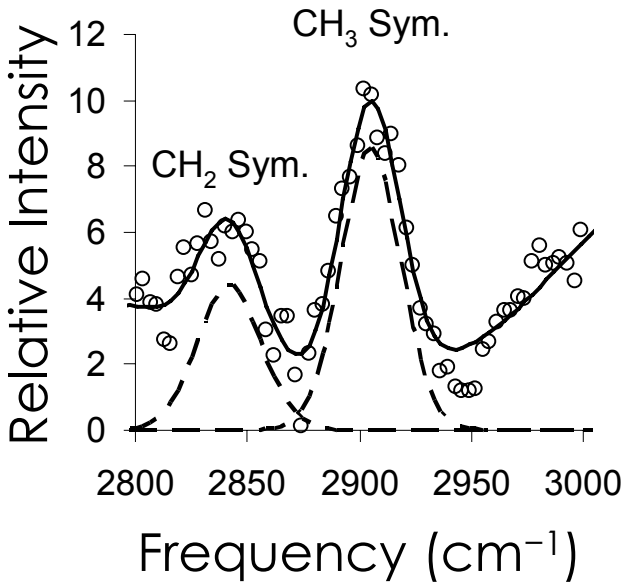

Figure 4A SFG spectra of a monomeric C18 sample under water at ambient pressure. The band to the left, centered at 2850 cm^{-1}, is the symmetric methylene stretch, and the band to the right, centered at 2910 cm^{-1}, is the symmetric methyl stretch.

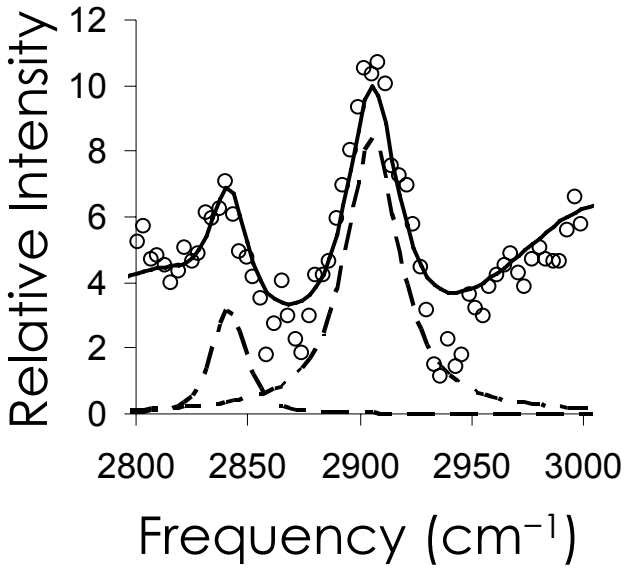

Figure 4B SFG spectra of a monomeric C18 sample under water at 20 atm.

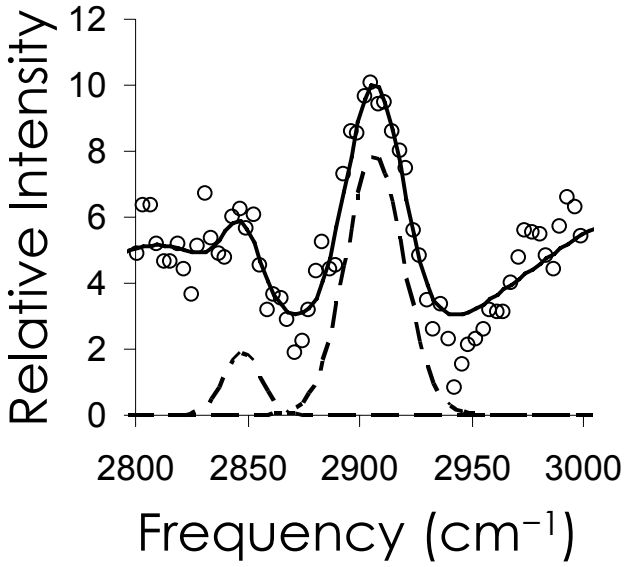

Figure 4C SFG spectra of a monomeric C18 sample under water at 40 atm.

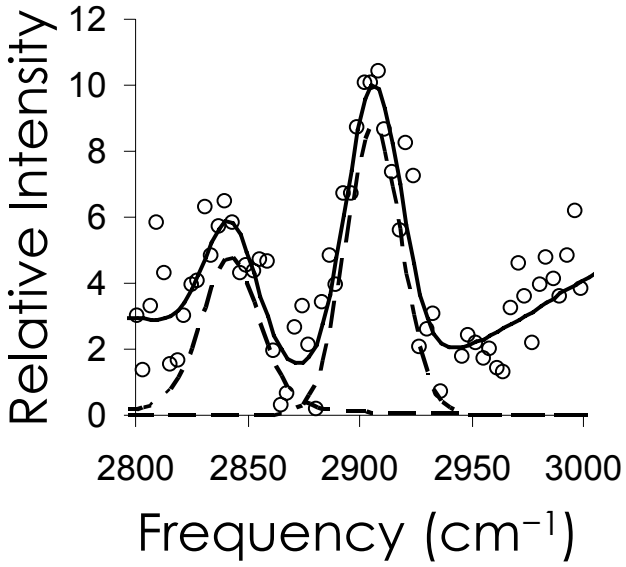

Figure 4D SFG spectra of a monomeric C18 sample under water at 60 atm.

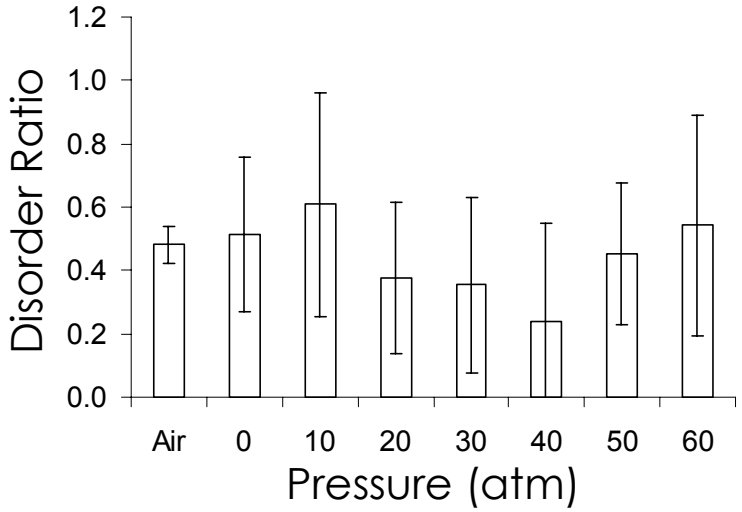

Figure 5 Disorder ratio of a monomeric phase sample in air and under water as a function of pressure. The disorder ratio is defined as the relative intensity of the symmetric methylene stretch to the symmetric methyl stretch. This provides a qualitative measure of the conformational disorder of the alkyl chains. The error bars represent 95% confidence intervals.

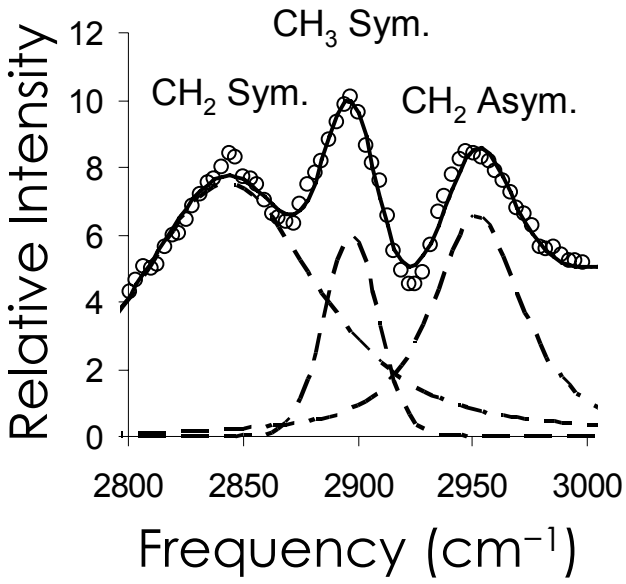

Figure 6A SFG spectra of a polymeric C18 sample under water at ambient pressure. The band to the left, centered at 2850 cm^{-1}, is the symmetric methylene stretch; the middle band, centered at 2910 cm^{-1}, is the symmetric methyl stretch; and the band to the right, centered at 2950 cm^{-1}, is the asymmetric methylene stretch.

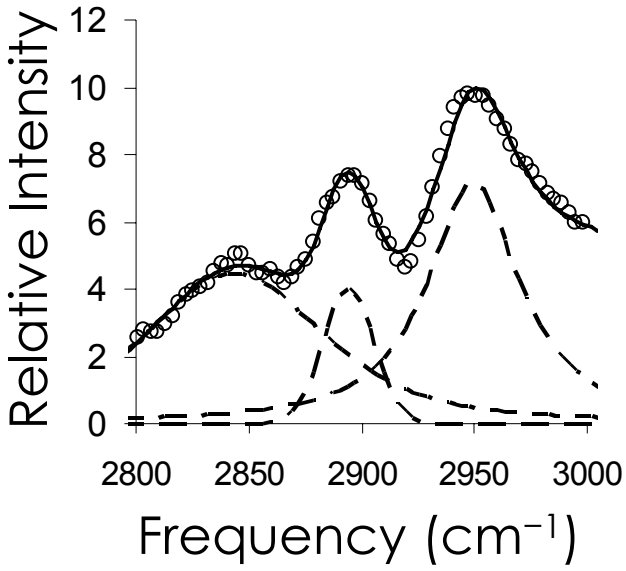

Figure 6B SFG spectra of a polymeric C18 sample under water at 20 atm.

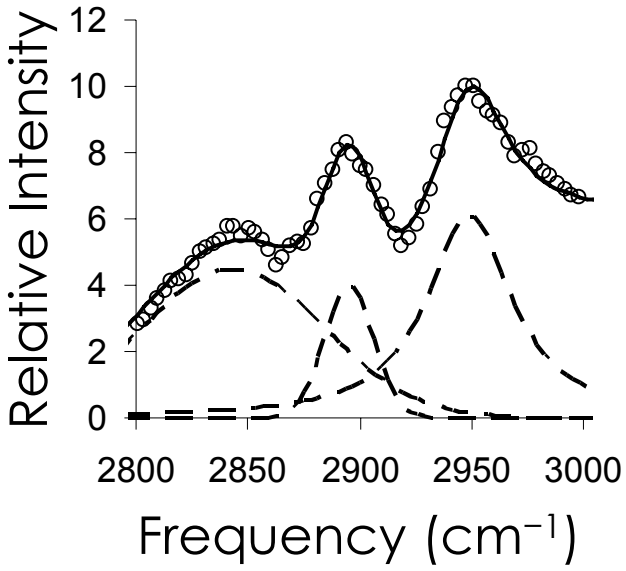

Figure 6C SFG spectra of a polymeric C18 sample under water at 40 atm.

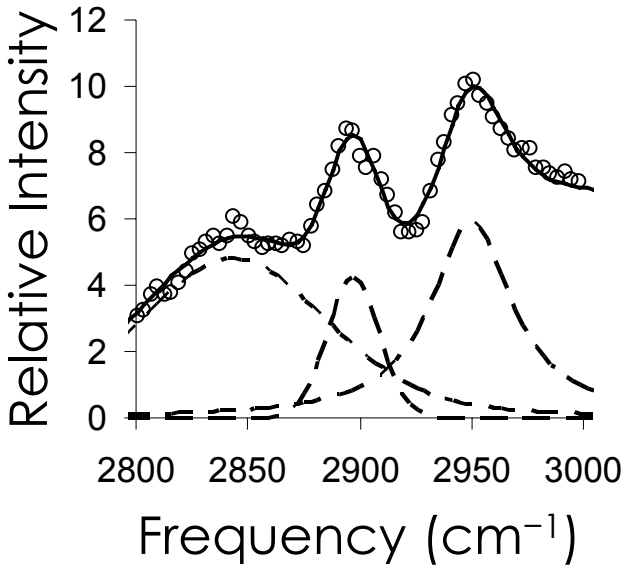

Figure 6D SFG spectra of a polymeric C18 sample under water at 60 atm.

Unlike spectra of the monomeric samples, the spectra in Figure 6 show a strong asymmetric methylene band in addition to the symmetric methyl band, suggesting that at least a portion of the chains are tilting toward the surface. I believe that this is a result of the difference in covalent structure between the monomeric and the polymeric samples. The polymeric samples consist of a random network of branched C18 chains due to the ability of the trichloro reagent to polymerize as well as attach to the silica substrate. Consequently, a distribution of chain orientations is observed in the polymeric samples, while the monomeric samples showed a more homogenous structural orientation. It seems likely that in water, the polymeric phase adopts a structure where the outer region of the film is similar to the monomeric phase samples in which the chains stand approximately normal to the sample surface, while the inner region of the film is more randomly oriented.

As pressure changes from ambient to 10 atm, the intensity of the asymmetric methylene band is shown to increase significantly; it then remains mostly constant with pressure up to 60 atm. This suggests that a collapse occurs in the polymeric phase under mild pressure in which the chains tilt toward the surface. This makes sense in terms of the mechanical effects of pressure which would cause the chains to lie down to minimize volume. Figure 7 shows the disorder ratios for the polymeric sample spectra. Going from air to water, significant ordering appears to occur in the alkyl chains of the polymeric phase. In water, pressure does not seem to have a significant effect on the disorder ratio.

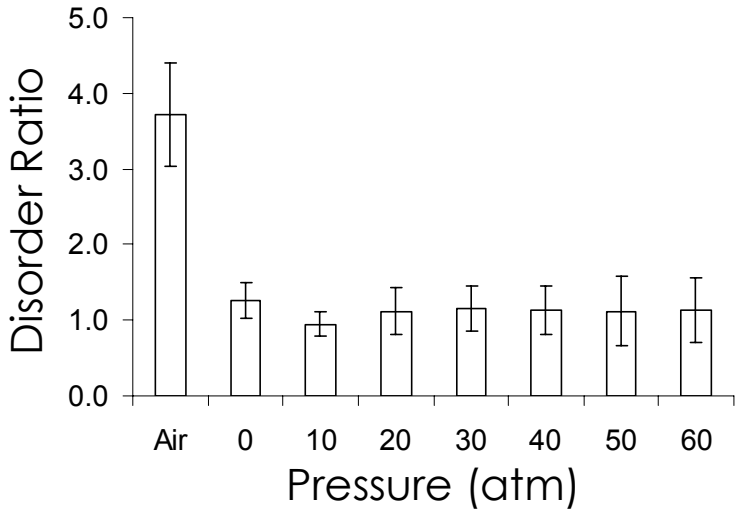

Figure 7 Disorder ratio of a monomeric phase sample in air and under water as a function of pressure. The disorder ratio is defined as the relative intensity of the symmetric methylene stretch to the symmetric methyl stretch. This provides a qualitative measure of the conformational disorder of the alkyl chains. The error bars represent 95% confidence intervals.

Conclusions

I obtained SFG spectra of monomeric and polymeric C18 models at the silca-air interface and at the silca-water interface. I observed that in both the monomeric and polymeric samples, the alkyl chains tend to lie down toward the surface in air, and to stand upright when placed in water. The polymeric phase samples are also shown to be much more ordered in water than in air. These observations are likely a result of entropic forces in the aqueous solvent that cause the non-polar stationary phase to adopt a conformation of minimum surface area at the polar interface. In water, the structure of the polymeric samples appears to be a distribution of orientations, with the chains at the outer surface of the film standing upright and the chains in the inner portion of the film showing greater disorder. The monomeric samples show a more homogenous structure with a greater degree of order.

I also demonstrated the ability to observe the structure of these model phases under pressure up to 60 atm. To the best of my knowledge, this represents the first direct measurement of stationary phase structure under pressure. The results show that mild pressure causes the alky chains in polymeric C18 phases to lie down toward the surface. After this pressure-induced conformational change occurs at about 10 atm, no further change in polymeric phase structure was observed with increasing pressure. The structure of the monomeric C18 model is shown to be unaffected by pressure up to 60 atm. It is important to note that this is a preliminary structural analysis and that a more rigorous treatment of the spectral data is forthcoming.

References

[1] W. Melander, Cs. Horvath, in Cs. Horvath (Editor), High-Performance Liquid Chromatography. Advances and Perspectives Vol. 2, Academic Press, New York, 1980.

[2] S.A. Wise, L.C. Sander, J. High Res. Chrom. & Chrom. Comm. 8 (1985) 248.

[3] R. Tijssen, P.J. Shoenmakers, M.R. Bohmer, L.K. Koopal, H.A.H. Billiet, J. Chromatogr. A. 656 (1993) 135.

[4] K.B. Sentell, J.G. Dorsey, Anal. Chem. 61 (1989) 930.

[5] C. Yan, D.E. Martire, Anal. Chem. 64 (1992) 1246, and papers cited therein.

[6] C. Yan, D.E. Martire, J. Phys. Chem 96 (1992) 3489.

[7] C. Yan, D.E. Martire, J. Phys. Chem 96 (1992) 3505.

[8] C. Yan, D.E. Martire, J. Phys. Chem 96 (1992) 7510.

[9] K.L. Williams, L.C. Sander, S.H. Page, S.A. Wise, HRC-J. High Res. Chrom. 18 (1995) 477.

[10] E. Martire, R.E. Boehm, J. Phys. Chem. 87 (1983) 1045.

[11] H. Lu, S.C. Rutan, Anal. Chem. 68 (1996) 1387.

[12] R.L. Pizzolatto, Y.L. Yang, L.K. Wolf, M.C. Messmer Anal. Chim. Acta 397 (1999) 81.

[13] Y. Liu, L.K. Wolf, M.C. Messmer, Langmuir 17 (2001) 4329.

[14] M.C. Henry, L.K. Wolf, M.C. Messmer, J. Phys. Chem. B 107 (2003) 2765.

[15] X. Li, M.C. Messmer, J. Chromatogr A 984 (2003) 19.

[16] M.C. Henry, E.A. Piagessi, J.C. Zesotarski, M.C. Messmer, Langmuir 21 (2005) 6521.

[17] B.A. Horn, Dissertation: Spectroscopic Investigation of Chromatographic Processes, Brigham Young University, Provo, UT, 2001.

[18] L.M. Ponton, S.M. Hoenigman, M. Cai, C.E. Evans, Anal. Chem. 72 (2000) 3581.

[19] F. Gritti, G. Felix, M.F. Achard, F. Hardouin, Chromatographia 53 (2001) 201.

[20] X.P. Li, V.L. McGuffin, J. Liq. Chromatogr. R. T. 30 (2007) 965.

[21] Z. Liao, C.J. Orendorff, J.E. Pemberton, Chromatographia 64 (2006) 139

Conclusions and Future Work

In this work, I used a number of spectroscopic techniques to probe mobile phase and stationary phase behavior under various chromatographic conditions. I have reported direct measurements of the mobile phase density in packed capillaries using Raman microspectroscopy, and this has allowed for accurate modeling of the flow behavior in compressible mobile phase separations. I have also analyzed on-column observations of analyte retention and separation efficiency using laser-induced fluorescence. This allowed me to correlate changes in separation speed and efficiency to local column conditions and provides a better understanding of the parameters governing column performance. Finally, I have probed the structure of monomeric and polymeric C18 models at elevated pressures. Observations of pressure-induced structural changes provide a basis for evaluating the effects of column pressure on shape selectivity. Together, this work provides a more complete understanding of the role of column pressure and fluid compressibility on the speed, efficiency, and selectivity of chemical separations.

Several questions have been raised in these studies that provide direction and ideas for future research. First, I have observed that in SGC, high temperature can help compensate for strong analyte retention near the column outlet caused by low mobile phase density. This observation suggests that operating an SGC column along an axial temperature gradient could linearize the rate of elution of less-volatile analyte. This technique would likely increase the speed of SGC and allow for analysis of larger compounds, and work is currently in progress to verify this hypothesis. As part of this experiment, it would also be useful to model the flow of the mobile phase in an SGC

column operating across an axial temperature gradient in addition to the isothermal flow profiles presented in this study.

I also noted that combining the column density gradient with a time-based program could allow for band focusing and sweeping for increased speed and peak capacity. This technique has promise for target analysis. I also believe that analogs could be developed to moving thermal gradients, used in GC, for supercritical fluid separations. Temperature programming and density gradient programming could be used as the time-based variable for peak sweeping. Use of a back-pressure regulated variable flow restrictor for density gradient programming is a promising area for further research.

Many researchers have observed a loss of efficiency with pressure drop in SFC. I observed a loss of efficiency in these experiments as well, and have hypothesized that this band broadening is caused by shearing of a film of CO_2 that forms in the stationary phase on the base of the silica packing. Verifying and characterizing this mechanism for band broadening is another area for future work. It is likely that SFG spectroscopy could be used to observe the formation of this film in a stationary phase model. Additionally, the concept of shearing suggests the possibility of dynamic behavior in the stagnant zone of the stationary phase. Probing the stagnant zone using SFG spectroscopy or fluorescence spectroscopy of an entrenched dye molecule under conditions of mobile phase flow would provide interesting insights to this question. The presence of radial temperature gradients in compressible mobile phase separations has also been suggested. In this work, I have looked only at axial column gradients. However, the development of spectroscopic techniques capable to probing radial column gradients stands to answer additional important questions.

Finally, the use of SFG to probe the effects of pressure on stationary phase structure can be applied to many other systems. Of particular interest is the effect of pressure on the structure of liquid crystals and cyclodextrins, which are often used for shape selective and chiral separations. In addition to probing the stationary phase, observing the orientation of partitioned analyte by SFG would provide further information about the retention mechanism of various stationary phase materials. This would be especially useful for proteins and peptides where the retention mechanism is poorly understood.